Annals of Nuclear Energy 208 (2024) 110778

Contents lists available at ScienceDirect

Annals of Nuclear Energy

journal homepage: www.elsevier.com/locate/anucene

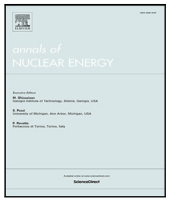

A new ^{181}Ta neutron resolved resonance region evaluation

D.P. Barry [a,*], M.T. Pigni [b], J.M. Brown [b], A.M. Lewis [a], T.H. Trumbull [a], K.H. Guber [b], B.J. McDermott [a], R.C. Block [c], Y. Danon [c]

[a] Naval Nuclear Laboratory, Schenectady, NY 12301, USA
[b] Oak Ridge National Laboratory, Oak Ridge, TN 37831, USA
[c] Rensselaer Polytechnic Institute, Gaerttner LINAC Center, Troy, NY 12180, USA

ARTICLE INFO

Keywords:
Tantalum
Neutron
Evaluation
Resolved
Resonance

ABSTRACT

A new ^{181}Ta neutron resolved resonance region evaluation has been performed from the thermal energy range up to approximately 2.5 keV. The R-matrix SAMMY code was used with the Reich–Moore approximation to evaluate resonance parameters from several experimental data sets. A Monte Carlo approach was used for resonance spin assignments and generating 59 small fictitious resonance levels which were shown to improve the cumulative level, Porter-Thomas, and Wigner distributions as compared to theoretical predictions. Covariance information was also generated for the entire resolved resonance region. The positive impact of the new evaluation was validated through benchmark calculations which were sensitive to the ^{181}Ta cross section and showed improvement in the reactivity bias for several benchmark cases.

1. Introduction

Tantalum is an important material that has potential uses in nuclear engineering applications such as being a control rod material in fast spectrum reactors (Tsubone et al., 1987; Shibata, 2016; McDermott et al., 2017) and a shielding material for fusion reactors (Tsubone et al., 1987). Tantalum is also used as a neutron production target in time-of-flight experiments (Danon et al., 1995). For these reasons, accurate tantalum neutron cross section data are important when researching and designing such nuclear systems. Due to its material properties such as a high melting point and corrosion resistance, tantalum can be used in plutonium casting operations (Chambers, 2022). The Nuclear Criticality Safety Program (NCSP) identified tantalum as an isotope of interest to be reevaluated in the resolved resonance region (RRR) (Chambers, 2022).

Since elemental tantalum is composed of 99.988% ^{181}Ta (Baum et al.), the evaluation presented in this paper concentrates only on this isotope and natural tantalum will effectively be treated as a ^{181}Ta mono-isotope.

1.1. Previous evaluations

The ^{181}Ta evaluation reported in the ENDF/B-VIII.0 library (Brown et al., 2018a), or ENDF-8.0 for brevity, appears to be one of the oldest RRR evaluations (Chambers, 2022). The ENDF-8.0 RRR parameter evaluation originates from ENDF-3.0 and only extends to 330 eV. The ENDF-3.0 evaluated parameters are based on the evaluation performed by Ottewitte et al. (1971) in 1971. Therefore, the current ENDF-8.0 evaluated RRR parameters for ^{181}Ta have remain unchanged for approximately 50 years.

The recent JENDL-5.0 contains an updated evaluation (Iwamoto et al., 2023) of the RRR parameters up to 150 eV. Above 150 eV, the RRR parameters were adopted from the JENDL-4.0 evaluation (Shibata et al., 2011), which has remained unchanged since the JENDL-3.2 evaluation (Nakagawa et al., 1995) performed in the mid nineties. The JENDL-5.0 RRR evaluation extends from thermal energy up to 2.4 keV.

The evaluated resonance parameters in JEFF-3.3 (Plompen et al., 2020) and JENDL-4.0 (Shibata et al., 2011) appear to be identical.

All of the aforementioned evaluations use a historical multi-level Breit–Wigner (MLBW) formalism (Herman and Trkov, 2010) which is now superseded by the Reich–Moore approximation of the R-matrix theory for use in modern evaluation work in the RRR for medium and heavy nuclei. Moreover, the previous ^{181}Ta evaluations are in need of considerable updates since they lack covariance information (uncertainty and correlations) for the resonance parameters.

For reasons such as these, a new ^{181}Ta RRR evaluation was performed which provides documentation, application of a modern R-matrix formalism, and covariance information for the RRR parameters.

The methods used to perform the present evaluation are discussed in Section 2, where Section 2.1 highlights the experimental data used and Section 2.2 gives the details of how the present evaluation was

* Corresponding author.
E-mail address: barryd3@rpi.edu (D.P. Barry).

https://doi.org/10.1016/j.anucene.2024.110778
Received 27 March 2024; Received in revised form 2 July 2024; Accepted 9 July 2024
Available online 28 July 2024

performed using the SAMMY (Larson, 2008) code. The results and discussion are given in Section 3, which includes the results of the SAMMY fits to the experimental data (Section 3.1), evaluated RRR parameters (Section 3.2), statistical distributions of the RRR parameters (Section 3.3), comparisons of the differential cross sections (Section 3.4), capture resonance integral and thermal cross sections (Section 3.5), thermal scattering values (Section 3.6), and the RRR parameter covariance (Section 3.7). The validation of the present RRR evaluation is covered in Section 4.

2. Evaluation methods

2.1. Experimental data used

The following sections will discuss the measured data used in the present evaluation work. The thermal energy range is defined up to 1 eV and the epithermal energy range is defined from 1 eV to 2.554 keV.

2.1.1. Thermal region

This energy region contains the important "thermal point" historically taken at 0.0253 eV and frequently used as an energy reference point when available in measured data.

A limited amount of useful ^{181}Ta thermal differential data were found in EXFOR (Otuka et al., 2014) including total and capture thermal cross section data sets from Malik et al. (1970) The differential thermal capture cross section data from Widder (1975) were also used.

Several thermal point capture data values (Malik et al., 1970; Seren et al., 1947; Pomerance, 1951; Prokhorov, 1956; Schmunk et al., 1960; Tattersall et al., 1960; Wolf, 1960; Markovic and Kocic, 1971; Takiue and Ishikawa, 1978; Heft, Mayaguez, 1978; Farina Arboccò et al., 2014) were obtained from EXFOR. These values were used to calculate an arithmetic average thermal point capture value of 20.88 ± 0.50 barns. It should be noted that some of the thermal point values were for natural Ta while others were for isotopic ^{181}Ta. Since the contribution of ^{180m}Ta at the thermal point is significantly less than the quoted uncertainties on the average value, the natural Ta and ^{181}Ta thermal point values were combined into a single set for a better statistical average.

The thermal elastic scattering point value was adopted from the National Institute of Standards and Technology (NIST) (National Institute of Standards and Technology (NIST) Center for Neutron Research, 2022; Sears, 1992) and had a value of 6.01 ± 0.12 barns.

The thermal total cross section was a derived quantity and was calculated by summing the capture and elastic thermal point values, giving 26.89 ± 0.51 barns.

2.1.2. Epithermal region

In this paper, the epithermal region is defined as the energy range from 1 eV to 2.554 keV which represents the upper energy range of the RRR region.

Among transmission data measured in the epithermal region, this evaluation used two experimental transmission data sets from Harvey et al. (1988) obtained directly from Oak Ridge National Laboratory (ORNL). These data are identical to those found in EXFOR but were grouped into a more convenient energy bin structure. Harvey's thin sample transmission data were used between 1–17 eV, while the thick sample transmission data were used between 17 eV and 2.554 keV.

For the capture reaction channel, neutron capture yield data measured using 2-mm and 6-mm-thick natural Ta samples by McDermott (2016) were available from the Gaerttner LINAC Center at Rensselaer Polytechnic Institute (RPI). These data were useful to fit resonance parameters in the low epithermal energy range from 1–155 eV.

An additional five experimental data sets measured by Brown (2019), Brown et al. (2018b) at the RPI facility were used in the epithermal energy range between 155 eV and 2.544 keV. These consisted of three neutron transmission data sets measured using 1 mm, 3 mm, and 6-mm-thick natural Ta samples. Two neutron capture yield data sets were available for 1-mm and 2-mm-thick samples.

The high resolution transmission data of Tsubone et al. (1987) are not currently reported in the EXFOR database and were not included in this evaluation work.

2.2. Details of SAMMY analysis

The SAMMY code (Larson, 2008) was used to fit R-matrix resonance parameters to the experimental data sets presented in Section 2.1. The intent of this new evaluation was to extend the current ENDF-8.0 ^{181}Ta RRR parameters from 330 eV to 2.554 keV.

Starting with the RRR parameter values from the JEFF-3.3 library, two new resonances at 1.9511 keV and 2.4596 keV were added as they were evident in the experimental data. The resonance spin assignments, J, were taken from the Atlas of Neutron Resonances (ATLAS-2018) (Mughabghab, 2018) when available. Unknown J values (not given in the ATLAS-2018) were determined using a Monte Carlo approach which was comprised of two stages.

In the first stage, all unknown J values were randomly sampled to create many sets of RRR parameters. Each random set of RRR parameters was compared to the theoretically predicted cumulative number of levels, Porter-Thomas, and Wigner distributions and an associated χ^2 value was calculated. The RRR parameter set that produced the lowest overall χ^2 value was deemed to be the best and the associated J values were chosen. Since this process produces a set of RRR parameters that best matches the predictions of the previously mentioned theoretical models, it is expected that the amount of misclassified J values was statistically minimized. The misclassification cannot be assessed on a resonance-by-resonance basis since this would require additional experimental information, which was not available.

The second stage of the Monte Carlo approach randomly added small fictitious resonances to each resonance spin group, J, in the set of RRR parameters with the lowest χ^2 values found in stage one. The fictitious resonances were created for each J spin group by randomly sampling the energy based on the average level spacing and the Γ_n based on the Porter-Thomas distribution. Resonance energies were added for both $J = 3$ and $J = 4$ starting above 700 eV. The work of Tsubone et al. (1987) suggested that small resonances were missing, especially below the Porter-Thomas statistic value below $x = \Gamma_n^0 / \langle \Gamma_n \rangle = 0.2$. Therefore, the random sampling of the Γ_n values from the Porter-Thomas distribution were biased to produce small resonances below $x \leq 0.2$. The updated RRR parameter set (after addition of small fictitious resonances) were compared to the theoretical distributions (cumulative levels, Porter-Thomas, Wigner) and the RRR parameter set that produced the lowest overall χ^2 was chosen as final. The second stage of the Monte Carlo approach generated 59 small fictitious resonances that improved the overall resonance statistics.

The thermal capture, scattering, and total values presented in Section 2.1.1 were used to constrain the SAMMY fitting process at 0.0253 eV. Two small negative bound levels were added to reproduce the thermal values as closely as possible. An arbitrary uncertainty of 0.1% was given to the thermal values to avoid instability in the fitting procedure due to the interference between long and short range correlations of the R-matrix model.

The s-wave potential scattering radius value of $R' = 7.86 \pm 0.24$ fm was found by taking the arithmetic average of the ENDF-8.0, JEFF-3.3, and ATLAS-2018 values. This calculated average agrees (within uncertainty) with the value found in the work of Brown (2019).

The R-matrix theory equations depend on the distant level term R^∞. It was decided to set R^∞ to zero during the SAMMY fitting processes. This entailed setting the value of the channel radius, a_c, equal to R' and have the R^∞ term represented using pairs of strong positive and negative distant resonances (Fröhner and Bouland, 2001) for each resonance spin, J. The use of distant resonances has an advantage

of being included in the calculation of the coherent and incoherent scattering values, which may serve as a validation check on the final RRR parameters.

The fit of the measured data presented in Section 2.1 was performed with the Bayesian procedure implemented in SAMMY up to 2.544 keV. A very small prior uncertainty (0.01%) was associated with the energy levels to guarantee stability in the fit, primarily for small resonances and regions where measured data show overlapping energy levels. In these cases, it can be difficult to identify resonance peaks and the fitted parameters may be inconsistent. Having the resonance levels almost treated as constants, the prior uncertainty on the capture and neutron widths was estimated to be 2% and 10%, respectively.

The SAMMY fitting process was performed sequentially. This means that a particular experimental data set was fit with SAMMY and the resulting RRR parameters and covariance outputs were used as inputs into the next experimental data SAMMY fit. This process allows each experimental data set to contribute to the overall fitting process. The final result of this sequential fitting process is a single set of RRR parameters (and corresponding covariance) that includes the effects of all of the fitted data. The SAMMY fits were sensitive to the order of the experimental data in the fitting process and it was necessary to start with transmission data first and then introduce the capture yield and various thermal cross section data later in the process.

The bound and distant level resonance parameters were not changed from their original values, but the prior uncertainties on these parameters were propagated into the final RRR parameters using the SAMMY Propagated Uncertainty Parameter (PUP) feature. Similarly, when possible, the uncertainties on experimental parameters, such as number density, burst width, effective temperature, background, and normalization, were also propagated into the final RRR parameters using the SAMMY PUP feature.

The SAMMY code also included multiple scattering, gamma attenuation, and weighting function corrections (McDermott, 2016; Brown, 2019) when needed for fitting experimental capture yield data.

The SAMMY free-gas model was used to perform Doppler broadening during the fitting procedure. The effective temperature of ^{181}Ta was determined to be 302.±6. K. This value was found by averaging the values obtained from two different methods. The first method (Moreh et al., 2006) gave an effective temperature value of 302.4 K and was calculated by integrating the phonon density of states (PDOS) spectrum of tantalum (Jani, 1985). The second method (Lamb, 1939) produced an effective temperature of 301.6 K based upon a Debye temperature of 225. K for tantalum (Ho et al., 1974). The uncertainty for the resulting average of these effective temperatures was assumed to be 2%.

Additional broadening effects are introduced into the transmission and capture yield data through various components of the neutron time-of-flight system used to perform the measurements. The major components that usually contribute to the experimental broadening effects are the LINAC electron burst width, time-of-flight channel widths, neutron target geometry, neutron moderator geometry, and the neutron detector geometry. These components were represented in SAMMY using analytical functions which were convoluted with the R-matrix model when fitting data to obtain the set of RRR parameters. The appropriate experimental resolution functions were obtained from the experimentalists who performed the transmission and capture yield measurements and are available upon request.

The RRR covariance information was generated using the SAMMY code and is discussed in Section 3.7. SAMMY was also used to convert the final covariance information into FILE32 using the LCOMP=1 format.

The RRR FILE2 parameters and associated FILE32 covariance were inserted into the most recent ENDF-8.0 file, with an updated FILE1 section, and uploaded to the NNDC GitLab repository.

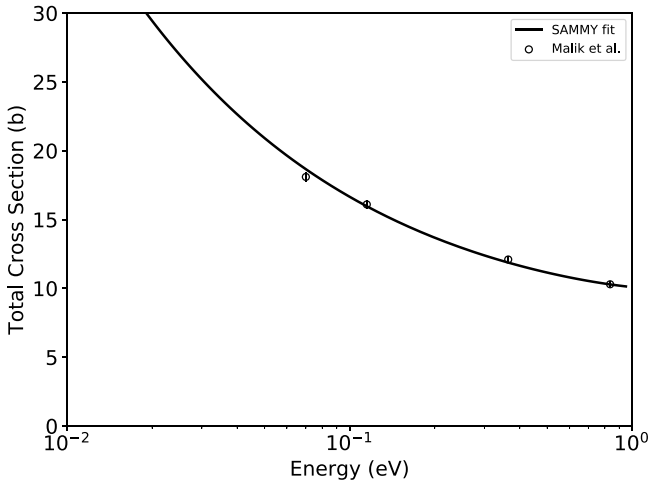

Fig. 1. Final SAMMY fits to the ^{181}Ta thermal total cross section data from Malik et al. (1970).

3. Results and discussion

The SAMMY code was used to fit relevant experimental data and evaluate RRR parameters. Examples of the quality of fitting are shown in Section 3.1 and a table of the new RRR parameters is reported in the Appendix A (Table A.1).

3.1. SAMMY fits to experimental data

The quality of SAMMY fits are exhibited in Figs. 1 through 6. The SAMMY fits to the experimental total and capture cross section thermal data are shown in Figs. 1 and 2, respectively. The SAMMY fits are in good agreement with the experimental thermal data cross sections.

The SAMMY fit to the experimental data for the 4.28 eV resonance is highlighted in Fig. 3. The SAMMY fit is in excellent agreement with the ORNL thin-sample transmission data, as well as producing a reasonably good fit to the RPI 2-mm-thick and 6-mm-thick capture yield data. It should be noted that the capture yield is not equal to unity since this is not a 100% capturing resonance.

Fig. 4 shows high quality SAMMY fitting to all of the available transmission and capture yield data in the energy region from 19 eV to 26 eV. These fits show excellent agreement with the ORNL thick-sample data and the RPI 2-mm-thick and 6-mm-thick capture yield data. Several thick-sample transmission data points with extremely large uncertainty due to the saturated resonance at about 24 eV generating nearly zero transmission data were removed from this figure for clarity.

Fig. 5 shows SAMMY fits to the transmission and capture yield experimental data between 210 eV and 240 eV. The transmission fits are very good. The capture fits to the RPI 1-mm-thick capture yield data are in reasonable agreement. However, the RPI 2-mm-thick capture yield data showed significant fluctuations which may be attributed to large variations in the flux counts exacerbated by the weighing function used in the data reduction process. The SAMMY code appears to have ignored many of these large fluctuations.

The SAMMY fits in Fig. 6 shows a high level density region between 2300 eV and 2500 eV. The transmission and capture yield fits appear to be of high quality. Once again, the RPI 2-mm-thick capture yield data display significant fluctuation.

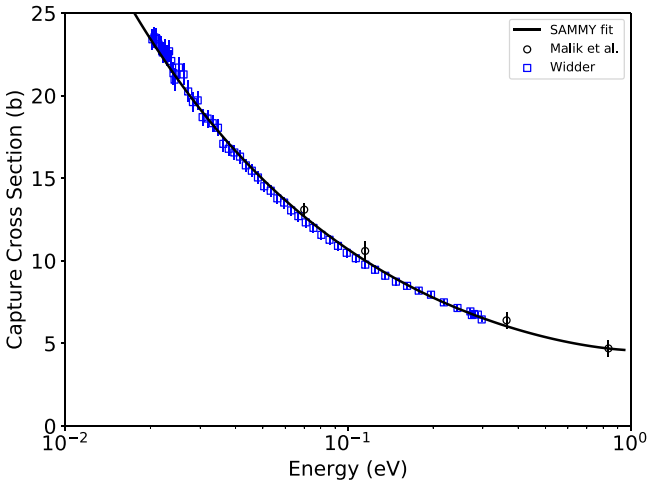

Fig. 2. Final SAMMY fits to the ^{181}Ta thermal capture cross section data from Malik et al. (1970) and Widder (1975).

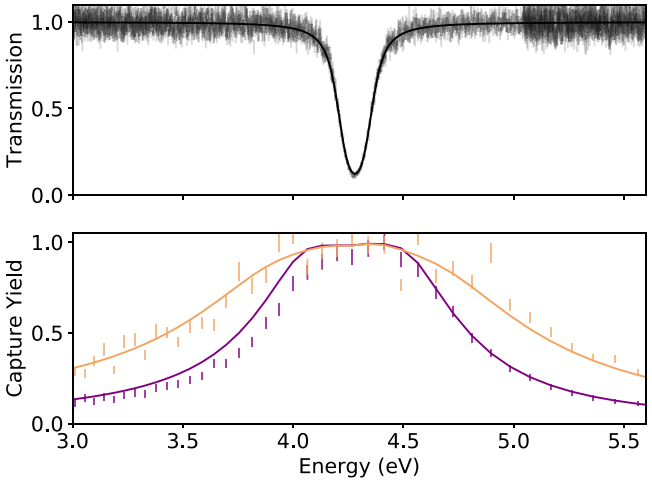

Fig. 3. The lowest positive energy ^{181}Ta resonance plotted in the energy region from 3.0 eV to 5.6 eV. The ORNL thin-sample transmission data (Harvey et al., 1988) (black points) are shown on the top. The RPI 2-mm-thick (purple points) and RPI 6-mm-thick (yellow points) capture yield data (McDermott, 2016) are shown on the bottom. The solid lines represent the SAMMY fits to these data.

3.2. Resolved resonance parameters

The SAMMY code was used to evaluate resonance parameters from fits to experimental data (Section 3.1). The RRR parameters can be found in Table A.1. The present evaluation extends the RRR region to an upper limit 2.554 keV. ^{181}Ta only has s-wave ($\ell = 0$) resonances in the RRR region. A pair of distant levels was added for each spin group ($J = 3$ and $J = 4$) to represent the R_0^{∞} term. A total of 59 small fictitious resonances were added to improve resonance statistics and are denoted using an asterisk symbol in Table A.1.

3.3. Resonance parameter distributions

3.3.1. Cumulative number of resonances

The cumulative number of resonances is expected to be linear with increasing energy if there are no missing or excess resonances. The cumulative number of positive ^{181}Ta resonance levels is plotted up to 2.554 keV for resonances with spin $J = 3$ and $J = 4$ in Figs. 7 and 8, respectively. The cumulative number of levels for the ENDF-8.0 evaluation stops at 330 eV. All of the plotted evaluations appear to be

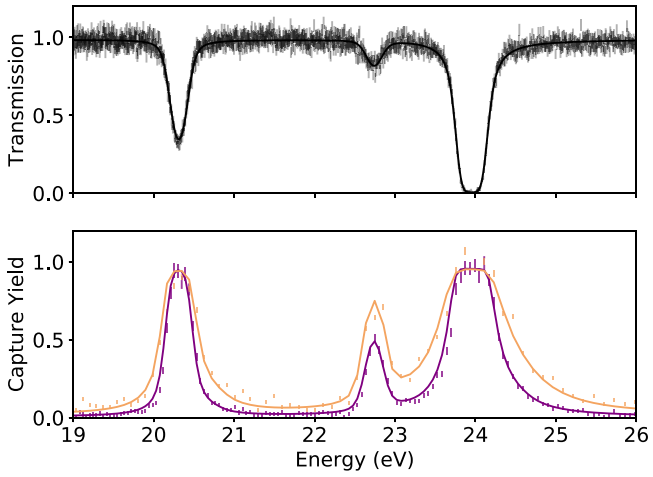

Fig. 4. ^{181}Ta resonances plotted in the energy region from 19.0 eV to 26.0 eV. The ORNL thick-sample transmission data (Harvey et al., 1988) (black points) are shown on the top. Several thick-sample data points with extremely large uncertainty due to the saturated resonance at about 24 eV generating nearly zero transmission data were removed from the figure for clarity. The RPI 2-mm-thick (purple points) and RPI 6-mm-thick (yellow points) capture yield data (McDermott, 2016) are shown on the bottom. The solid lines represent the SAMMY fits to these data.

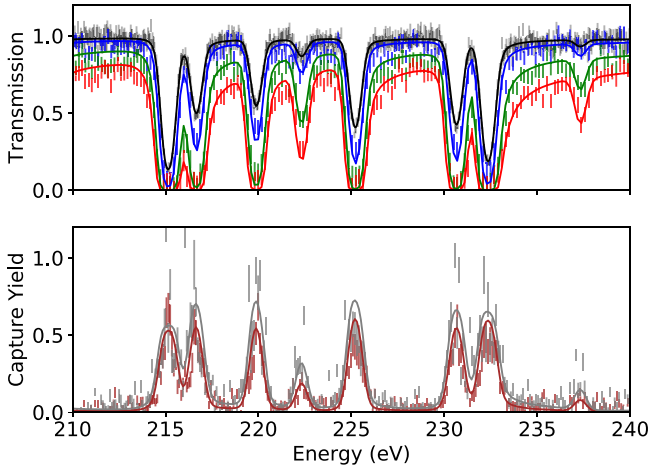

Fig. 5. ^{181}Ta resonances plotted in the energy region from 210.0 eV to 240.0 eV. The top plot shows the transmission data for the ORNL thick-sample (Harvey et al., 1988) (black points). In addition, the top plot also shows the RPI 1-mm-thick (blue points), 3-mm-thick (green points), and 6-mm-thick (red points) transmission data (Brown, 2019). The lower plot shows the RPI 1-mm-thick (brown points) and 2-mm-thick (gray points) capture yield data (Brown, 2019). The solid lines represent the SAMMY fits to these data.

linear up to 330 eV. The JEFF-3.3 and JENDL-5.0 evaluations produce almost identical results for both $J = 3$ and $J = 4$ resonance spin groups. The JEFF-3.3 and JENDL-5.0 evaluations deviate from linearity for $J = 3$ between approximately 1250 eV and 1800 eV and appear to have an excess of levels. This excess of levels may be attributed to a possible misassignment of some J spin values. For the $J = 4$ resonance group, the JEFF-3.3 and JENDL-5.0 evaluations deviate from linearity above approximately 1000 eV and appear to be missing levels above this energy. The present evaluation produces a more linear shape for the entire RRR energy range, indicating that the new spin assignments are reasonable (i.e., low misclassification) and any missing or extra levels may not noticeable. The present evaluation is expected to have less misclassification due to the statistical process described in Section 2.2. In addition, the present evaluation also has the expected number of resonances for each J value, which is expected to be proportional to $2J+1$.

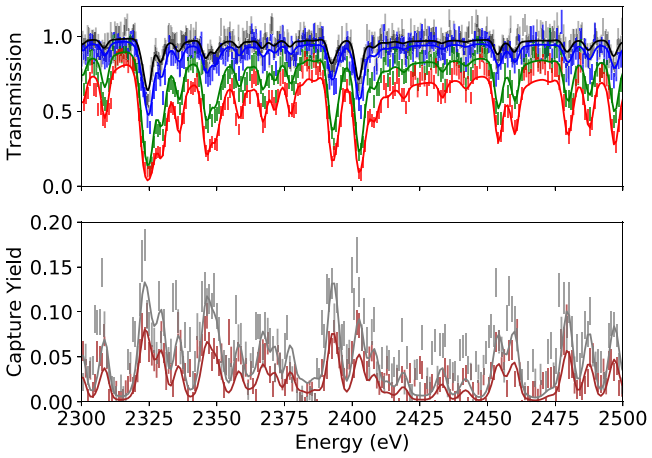

Fig. 6. ^{181}Ta resonances plotted in the energy region from 2300.0 eV to 2500.0 eV. The top plot shows the transmission data for the ORNL thick-sample (Harvey et al., 1988) (black points). In addition, the top plot also shows the RPI 1-mm-thick (blue points), 3-mm-thick (green points), and 6-mm-thick (red points) transmission data (Brown, 2019). The lower plot shows the RPI 1-mm-thick (brown points) and 2-mm-thick (gray points) capture yield data (Brown, 2019). The solid lines represent the SAMMY fits to these data.

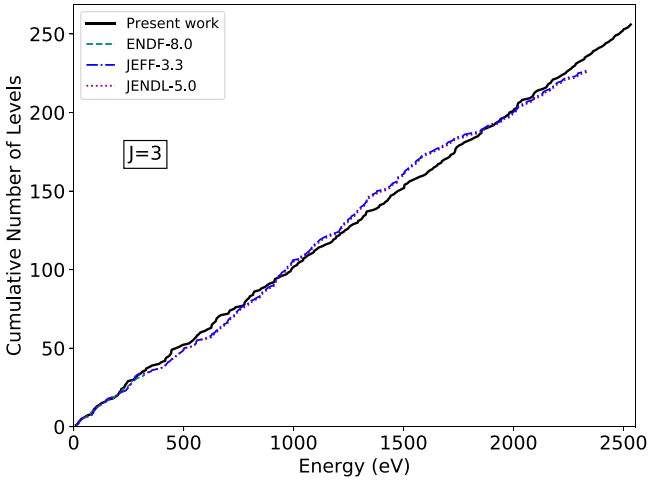

Fig. 7. Cumulative number of resonance levels for the present ^{181}Ta $J = 3$ s-wave ($\ell = 0$) RRR parameters as compared to ENDF-8.0, JEFF-3.3, and JENDL-5.0. Only positive energy resonance levels up to 2.554 keV were used. ENDF-8.0 only goes up to 330 eV and any differences between evaluations are unnoticeable in this small energy region. The JEFF-3.3 and JENDL-5.0 evaluations are on top of each other.

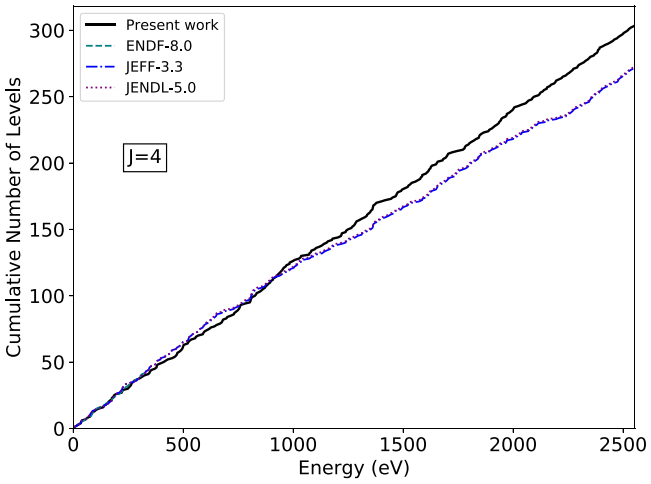

Fig. 8. Cumulative number of resonance levels for the present ^{181}Ta $J = 4$ s-wave ($\ell = 0$) RRR parameters as compared to ENDF-8.0, JEFF-3.3, and JENDL-5.0. Only positive energy resonance levels up to 2.554 keV were used. ENDF-8.0 only goes up to 330 eV and any differences between evaluations are unnoticeable in this small energy region. The JEFF-3.3 and JENDL-5.0 evaluations are on top of each other.

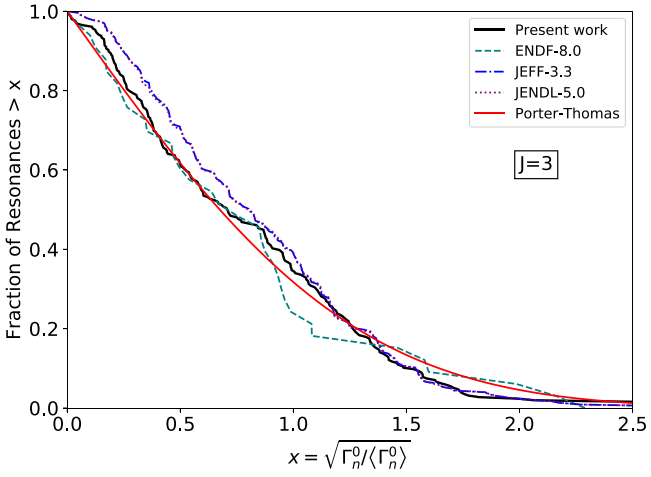

Fig. 9. Cumulative fractional distribution of reduced neutron widths for the present ^{181}Ta s-wave ($\ell = 0$) $J = 3$ RRR parameters. Also shown for comparison are the ENDF-8.0, JEFF-3.3, JENDL-5.0, and theoretical Porter-Thomas distributions. The present work more closely matches the Porter-Thomas distribution. Only positive energy resonance levels up to 2.554 keV were used.

3.3.2. *Reduced neutron width distribution*

The distribution of the reduced neutron widths is plotted for resonances in the RRR energy range with spin $J = 3$ and $J = 4$ in Figs. 9 and 10, respectively. The ENDF-8.0 evaluation agrees well with the theoretical Porter-Thomas distribution but has more fluctuations due to the resonances region being limited to below 330 eV. The JEFF-3.3 and JENDL-5.0 have almost identical results but appear to be lacking resonances with smaller reduced neutron widths. When compared to the JEFF-3.3 and JENDL-5.0 evaluations, the present evaluation improves the reduced neutron width distributions and more closely follows the theoretical Porter-Thomas distribution.

3.3.3. *Resonance spacing distribution*

The ^{181}Ta resonance level spacing distributions are plotted for spins $J = 3$ and $J = 4$ in Figs. 11 and 12, respectively. The ENDF-8.0 evaluation appears to agree relatively well with the theoretical Wigner distribution, but has larger fluctuations due to the smaller number of resonances (limited to below 330 eV). The resonance spacing distributions for the JEFF-3.3 and JENDL-5.0 evaluations are almost identical to each other. As compared to JEFF-3.3 and JENDL-5.0 the present evaluation more closely matches the theoretical Wigner distribution.

3.4. *Differential cross section comparisons*

For overall comparisons, all of the investigated evaluations were converted to point-wise cross section and Doppler broadened to 293.6 K (room temperature) using the NJOY (Macfarlane et al., 2017) code.

Fig. 13 shows the total, capture, and elastic thermal cross section shapes between 0.02 eV and 0.05 eV. The present evaluation produces cross sections in this energy region that are visibly lower than ENDF-8.0 and higher than both JEFF-3.3 and JENDL-5.0. The cross section values at the thermal energy point (0.0253 eV) are discussed in Section 3.5.

Fig. 14 shows the total, capture, and elastic cross sections for the lowest energy resonance near 4.3 eV. The present evaluation produces higher peak cross section at 4.3 eV relative to JEFF-3.3. In contrast,

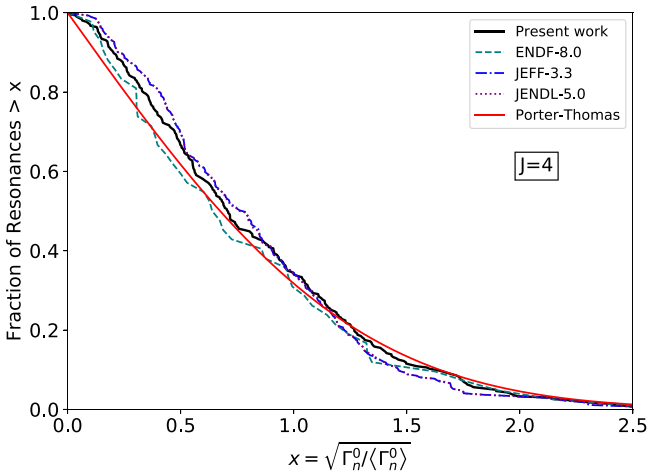

Fig. 10. Cumulative fractional distribution of reduced neutron widths for the present ^{181}Ta s-wave ($\ell = 0$) $J = 4$ RRR parameters. Also shown for comparison are the ENDF-8.0, JEFF-3.3, JENDL-5.0, and theoretical Porter-Thomas distributions. The present work more closely matches the Porter-Thomas distribution. Only positive energy resonance levels up to 2.554 keV were used.

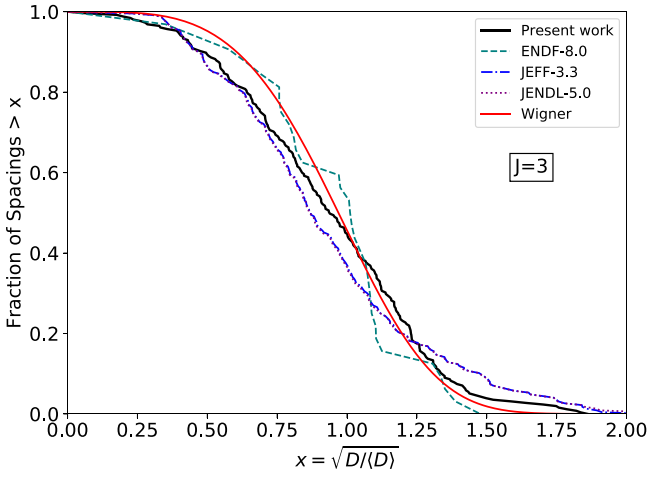

Fig. 11. Cumulative fractional distribution of resonance spacing for the present ^{181}Ta s-wave ($\ell = 0$) $J = 3$ RRR parameters. Also shown for comparison are the ENDF-8.0, JEFF-3.3, JENDL-5.0, and theoretical Wigner distributions. The present work more closely matches the Wigner distribution. Only positive energy resonance levels up to 2.554 keV were used.

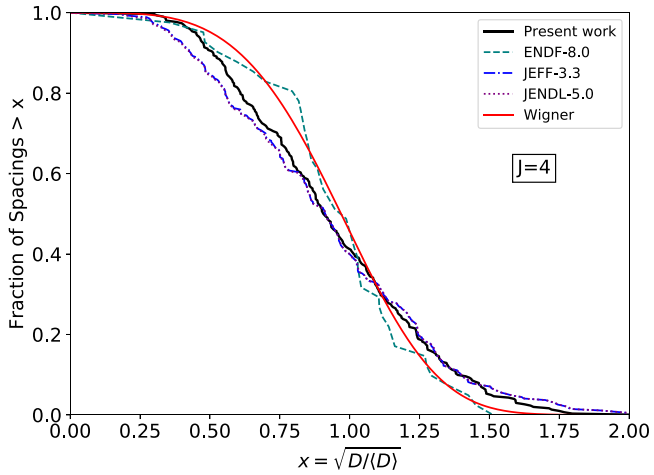

Fig. 12. Cumulative fractional distribution of resonance spacing for the present ^{181}Ta s-wave ($\ell = 0$) $J = 4$ RRR parameters. Also shown for comparison are the ENDF-8.0, JEFF-3.3, JENDL-5.0, and theoretical Wigner distributions. The present work more closely matches the Wigner distribution. Only positive energy resonance levels up to 2.554 keV were used.

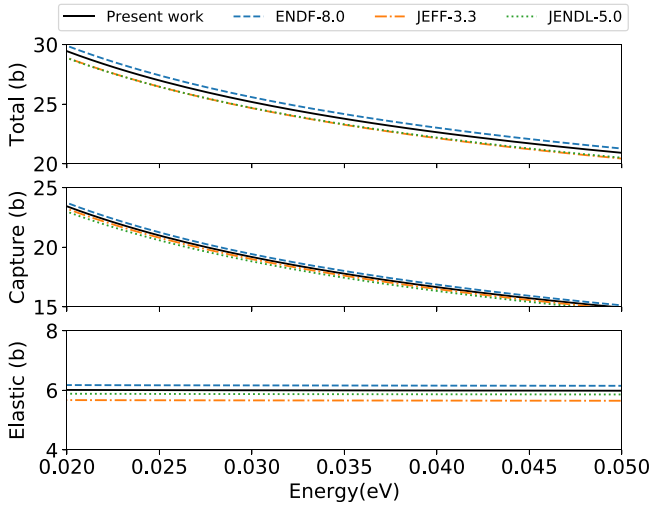

Fig. 13. Comparison of the ^{181}Ta differential total (top), capture (middle), and elastic scattering (bottom) cross sections in the thermal energy region from 0.02 eV to 0.05 eV. The cross sections were reconstructed and broadened to room temperature (293.6 K) using NJOY.

the present evaluation produces a lower peak cross section at 4.3 eV relative to ENDF-8.0 and JENDL-5.0. These differences in the 4.3 eV resonance have a large impact on the resonance integral values given in Table 1.

The total, capture, and elastic cross sections between 300 eV and 350 eV are shown in Fig. 15. It is evident that the ENDF-8.0 RRR evaluation ends at 330 eV, after which no more resonance structure exists. The present RRR evaluation shows significant differences compared to ENDF-8.0, JEFF-3.3 and JENDL-5.0 in the lower part of this energy region.

Lastly, the cross sections are plotted in Fig. 16 between 2.3 keV and 2.554 keV. The present RRR evaluation extends further than JEFF-3.3 and JENDL-5.0, which both end at 2.4 keV. The RRR for the present evaluation extends to 2.554 keV.

3.5. Capture resonance integral and thermal cross sections

The room temperature (293.6 K) point-wise cross sections were reconstructed for all investigated evaluations using the NJOY code (Section 3.4). The capture cross sections were used to calculate the resonance integral, RI_γ, for each evaluation using the INTER code, which performed the following integration:

$$RI_\gamma = \int_{0.5\text{eV}}^{100\text{keV}} \frac{\sigma_x(E)}{E} dE \quad . \tag{1}$$

It should be noted that the upper integration limit was kept at the INTER default value of 100 keV as it corresponded to the end of the Unresolved Resonance Region (URR) that was being performed (Brown et al., 2024) in conjunction with the present RRR evaluation.

The resulting RI_γ values are presented in Table 1. The present RI_γ value differs from most of the other investigated evaluations. The notable exception being relatively good agreement with the JENDL-5.0 evaluation. The RI_γ for the present evaluation is ≈4% lower than ENDF-8.0, ≈7% higher than JEFF-3.3, and ≈1% higher than JENDL-5.0. The present RI_γ value is also ≈8% higher than that given by the neutron ATLAS-2018.

Eq. (1) shows that the RI_γ calculation weights the cross section by $1/E$. This means that the lowest energy resonances can have the largest

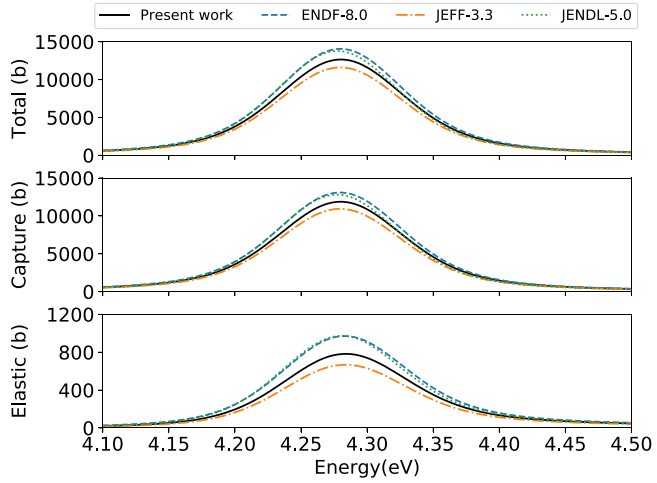

Fig. 14. Comparison of the ^{181}Ta differential total (top), capture (middle), and elastic scattering (bottom) cross sections for the strong low energy resonance between 4.1 eV to 4.5 eV. The cross sections were reconstructed and broadened to room temperature (293.6 K) using NJOY.

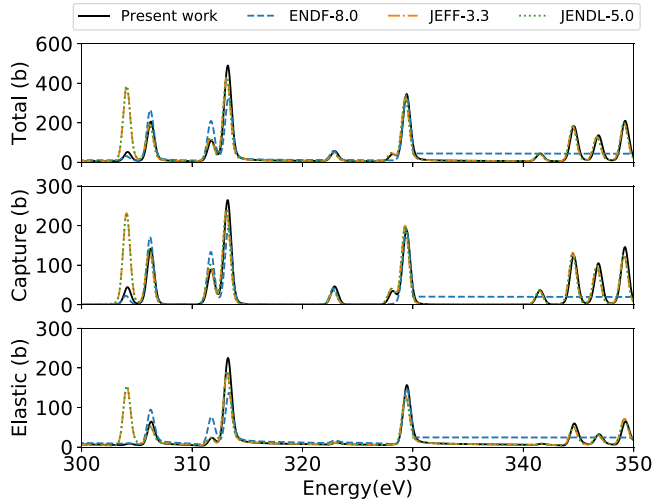

Fig. 15. Comparison of the ^{181}Ta differential total (top), capture (middle), and elastic scattering (bottom) cross sections in the energy region from 300 eV to 350 eV. Differences in some peak cross sections between 300 eV and 320 eV are evident. The ENDF-8.0 RRR ends at 330 eV. The cross sections were reconstructed and broadened to room temperature (293.6 K) using NJOY.

impact on the RI_γ value. Therefore, the differences between the RI_γ values are largely influenced by the changes in the 4.28 eV resonance parameters which contribute approximately 60% to the integral and produce a significant change in the resulting cross section (see Fig. 14).

The INTER code was also used for the reconstruction of the cross sections calculated at the thermal energy of 0.0253 eV and room temperature (293.6 K). Reported in Table 1, the present thermal cross section values agree with most of the investigated evaluations within the quoted uncertainties. A small difference is noticed when comparing the present and JEFF-3.3 thermal scattering cross sections. In addition, the present thermal capture and scattering cross section values agree with the ATLAS-2018 and NIST values within the quoted uncertainty.

The uncertainty on the thermal cross section values were calculated using the ERROR and COVR modules in NJOY with a small energy group centered around the thermal energy at 0.0253 eV. This allowed for the propagation of covariance into these calculated values.

The evaluated RI_γ uncertainty presented in this work was calculated using a Monte Carlo process, in which the present RRR parameters

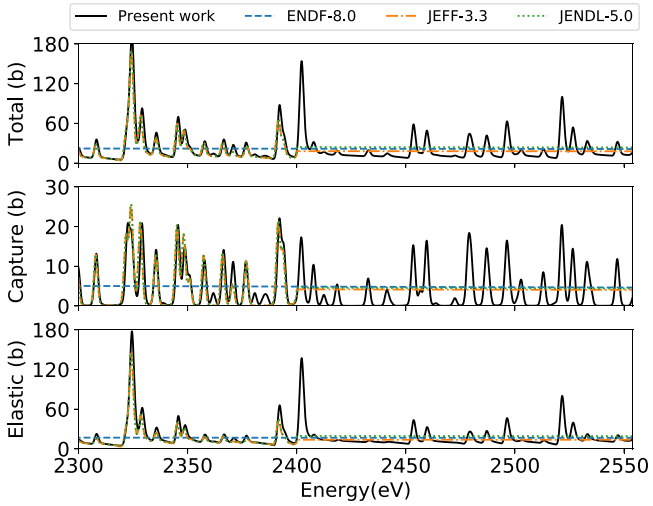

Fig. 16. Comparison of the ^{181}Ta differential total (top), capture (middle), and elastic scattering (bottom) cross sections in the energy region from 2300 eV to 2554 eV. The ENDF-8.0 RRR ends at 330 eV and has no structure in this higher energy region. The RRR for the JEFF-3.3 and JENDL-5.0 evaluations end at 2.4 keV. The cross sections were reconstructed and broadened to room temperature (293.6 K) using NJOY.

(Table A.1) were randomly sampled based on their uncertainty to create an adjusted evaluation file. This adjusted evaluation file was then processed with NJOY and INTER to get a corresponding RI_γ value. This process was repeated over 700 times, resulting in an array of RI_γ values. The standard deviation of this array of values was taken to be the uncertainty on the RI_γ value in Table 1. It should be noted that covariance information was not used when randomly sampling the RRR parameters.

3.6. Coherent and incoherent thermal scattering values

The free scattering length for a set of s-wave ($\ell = 0$) resonances with a particular spin J can be calculated using a summation of resonance parameters as follows (Mughabghab, 2018)

$$a = R' - 2.227 \times 10^3 \left(\frac{A+1}{A}\right) \sum_J \frac{\Gamma^0_{n,J}}{E_{r,J}} \quad , \tag{2}$$

where R' is the potential scattering radius, A is the ratio of the target mass with respect to the neutron mass (i.e., $m_{target}/m_{neutron}$), $\Gamma^0_{n,J}$ is the reduced neutron width, and $E_{r,J}$ is the resonance energy. Since ^{181}Ta has two spin states ($J = 3$, $J = 4$), the coherent scattering length, a_{coh}, can be found using the following combination

$$a_{coh} = g_- a_- + g_+ a_+ \quad , \tag{3}$$

where $g = (2J+1)/(2(2I+1))$ is the statistical spin factor and the + and − subscripts signify the $J = 3$ and $J = 4$ spin states, respectively.

Similarly, the incoherent scattering length, a_{inc}, can be found using a combination of resonance spin states as follows

$$a_{inc} = \sqrt{g_- g_+}\,(a_+ - a_-) \quad . \tag{4}$$

The free coherent, a_{coh}, and free incoherent, a_{inc}, scattering lengths were converted to bound coherent, b_{coh}, and bound incoherent, b_{inc}, scattering lengths by correcting for center of mass

$$b_x = \left(\frac{A+1}{A}\right) a_x \quad , \tag{5}$$

where x signifies *coh* or *inc*.

The bound scattering lengths can generally be measured precisely with an experiment. Therefore, the bound scattering lengths calculated

Table 1
Thermal value results from NJOY and INTER. The bound coherent and incoherent thermal scattering values were calculated using the equations shown in Section 3.6. The NIST values and uncertainties originate from Sears (1992). All uncertainties provided represent 1σ.

	Present Work	ENDF-8.0	JEFF-3.3	JENDL-5.0	ATLAS-2018	NIST
σ_t^0 (b)	26.9 ± 0.7	27.3	26.3	26.3	–	–
σ_γ^0 (b)	20.9 ± 0.5	21.1	20.7	20.5	20.4 ± 0.3	20.5 ± 0.5
σ_s^0 (b)	6.0 ± 0.2	6.2	5.7	5.9	6.14 ± 0.15	6.01 ± 0.12
RI_γ (b)	710.±3.	738.5	659.4	715.7	655 ± 20	–
R′ (fm)	7.86 ± 0.24	8.1271	7.8	7.8	7.65 ± 0.20	–
b_{coh} (fm)	6.94 ± 0.19	6.97	6.74	6.87	6.91 ± 0.07	6.91 ± 0.07
b_{inc} (fm)	−0.29 ± 0.18	−0.98	−0.25	0.22	–	−0.29 ± 0.03

Table 2
The benchmark and calculated results for PMM003 using ^{181}Ta evaluations from the present work, ENDF-8.0, JEFF-3.3, and JENDL-5.0. The benchmark k_{eff} is given with 1σ uncertainty and the MCNP calculated k_{eff} is given with a 95% confidence interval (CI). The calculated energy of average neutron lethargy causing fission (EALF) is given in units of MeV. For comparisons, the value $C/E-1$ is presented where C and E represents the MCNP calculated k_{eff} and published benchmark k_{eff}, respectively.

PMM003	Benchmark		Present Work			
Case No.	k_{eff}	1σ	k_{eff}	95% CI	EALF	C/E-1
1	0.99953	0.00195	1.00985	0.00020	1.0249E−1	0.01032
2	0.99938	0.00154	1.00612	0.00020	1.6527E−2	0.00674
3	1.00008	0.00154	1.00459	0.00024	8.6769E−4	0.00451
4	1.00078	0.00142	1.00117	0.00024	3.3215E−5	0.00092
5	0.99871	0.00121	0.99964	0.00012	2.9471E−6	0.00093
PMM003	Benchmark		ENDF-8.0			
Case No.	k_{eff}	1σ	k_{eff}	95% CI	EALF	C/E-1
1	0.99953	0.00195	1.00956	0.00022	1.0259E−1	0.01003
2	0.99938	0.00154	1.00771	0.00022	1.6386E−2	0.00834
3	1.00008	0.00154	1.00720	0.00022	8.5769E−4	0.00712
4	1.00078	0.00142	1.00272	0.00024	3.3099E−5	0.00194
5	0.99871	0.00121	0.99952	0.00024	2.9528E−6	0.00081
PMM003	Benchmark		JEFF-3.3			
Case No.	k_{eff}	1σ	k_{eff}	95% CI	EALF	C/E-1
1	0.99953	0.00195	1.01639	0.00022	1.0302E−1	0.01687
2	0.99938	0.00154	1.01632	0.00020	1.6126E−2	0.01695
3	1.00008	0.00154	1.01493	0.00022	8.4136E−4	0.01485
4	1.00078	0.00142	1.00891	0.00024	3.2526E−5	0.00812
5	0.99871	0.00121	1.00423	0.00024	2.9241E−6	0.00553
PMM003	Benchmark		JENDL-5.0			
Case No.	k_{eff}	1σ	k_{eff}	95% CI	EALF	C/E-1
1	0.99953	0.00195	1.01063	0.00020	9.5045E−2	0.01111
2	0.99938	0.00154	1.01333	0.00020	1.0585E−2	0.01396
3	1.00008	0.00154	1.01458	0.00020	8.0660E−4	0.01450
4	1.00078	0.00142	1.01020	0.00022	3.1965E−5	0.00941
5	0.99871	0.00121	1.00561	0.00024	2.8912E−6	0.00691

from resonance parameters can be directly compared to the experimental result, in the present case the NIST value. The NIST value for b_{coh} from ^{181}Ta appears to have originated from the high quality experiments by Koester and Knopf (1971) and Koester et al. (1991)

The above equations were used to generate b_{coh} and b_{inc} using the resonance parameters in Table A.1. The resulting bound scattering length values are given in Table 1. The uncertainty on the present bound scattering lengths were obtained using the same Monte Carlo method explained previously in Section 3.5. The present evaluation gives a b_{coh} value that agrees with all of the investigated evaluations within the quoted uncertainty. The present b_{coh} is also in excellent agreement with the ATLAS-2018 and NIST values. The present b_{inc} value agrees with JEFF-3.3 within uncertainty, but disagrees with ENDF-8.0 and JENDL-5.0.

Since the NIST value is assumed to be correct, the present evaluation does the best job at reproducing the bound scattering values.

3.7. Resonance parameter covariance

The SAMMY code was used to generate the RRR parameter covariance matrix. To incorporate the overall fitting uncertainty, the reduced χ^2 values for all of the SAMMY fits to the experimental data sets were averaged and found to be 1.6. The FILE32 covariance matrix was then multiplied by the square of this value, 2.6. The resulting covariance matrix for total, capture, and elastic scattering are show in Figs. 17 through 19, respectively. These figures were generated using NJOY/ERRORR with a constant weighting function and grouping based on the SCALE 252-group structure (only taken for energies below the RRR limit of 2.554 keV).

Fig. 17 shows that, for this particular group structure, the baseline uncertainty on the total cross section decreases from approximately 3% to about 1% near 50 eV, and remains about 1% until the end of the RRR region at 2.554 keV. Fig. 18 shows that elastic scattering cross section follows a similar trend starting from approximately 5% and dropping to about 1% above 50 eV. Lastly, Fig. 19 shows that the radiative capture uncertainty starts around 2% and decreases to 1% near 300 eV, above which the lowest uncertainty regions drop to approximately 0.5%. These uncertainties depend on the chosen energy group structure. Particularly above 300 eV, by using a denser energy bin structure the average uncertainty can significantly increase. For example, changing the 305 eV to 550 eV bin width to a smaller 305 eV to 325 eV bin width increases the uncertainty on the radiative capture cross section from 0.4% to 1.6%. All of covariance plots show that the relative uncertainty exhibits strong fluctuations due to the underlying resonance structure.

The effect of the energy bin width on the grouped cross section uncertainty may be attributed to the magnitude and range of the correlations. As shown in Figs. 17–19, there appears to be large-magnitude and long-range uncertainty correlations up to about 100 eV. These large-magnitude long-range correlations are introduced by the low-energy wings of strong resonances (i.e., high peak cross sections). For neutron energies above 100 eV, due to the gradual reduction of resonance peaks and subsequent low-energy tails, the correlation matrices show primarily small-magnitude and short-range positive correlations. Particularly, in this energy region associated with small-magnitude short-range correlations, the uncertainty on the group cross section may be highly dependent on the energy group structure. At first glance, this may be interpreted as a lack of systematic uncertainty. However, more studies are needed to understand the systematic uncertainty related to experimental data used in the evaluation of the RRR parameters. Moreover, in the present and other R-matrix analyses, it seems the decreased correlation of the RRR parameter correlation matrix with increasing incident neutron energy may be related to the magnitude of the resonance levels. Although more study is needed, the reduction of the grouped uncertainty may be related to the natural decrease in cross section magnitude with increasing energy.

An option to include the effects of the experimental systematic uncertainty in FILE 33 was considered but resulted in a fully correlated covariance matrix and was, therefore, not used.

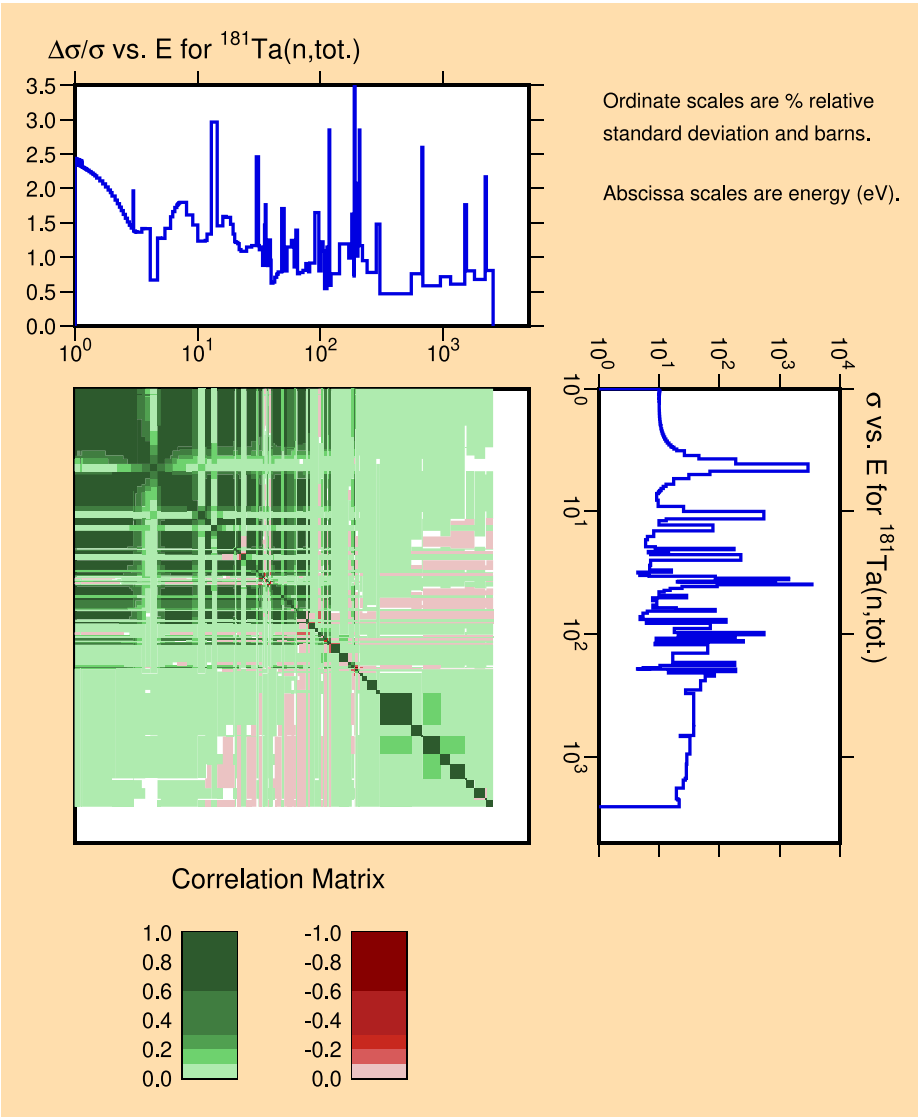

Fig. 17. The present ^{181}Ta total cross section covariance. These data were generated using NJOY/ERRORR with a constant weighting flux. The energy bins were based on the SCALE 252-group structure (only using the energies bins below the RRR limit of 2.554 keV).

4. Validation

Validation of the proposed changes to the ^{181}Ta RRR parameters was accomplished using the plutonium Thermal/Epithermal Experiment (TEX-Pu) with a tantalum diluent, adopted as PU-MET-MIXED-003 (PMM003) in the International Criticality Safety Benchmark Project (ICSBEP) Handbook (Bess et al., 2020), analyzed with MCNP6.2 (Werner et al., 2017). PMM003 consists of five cases with neutron energy spectra ranging from fast to thermal, based on the amount of moderator included in the benchmark, making this benchmark ideal for validating changes in the resolved resonance, unresolved resonance, and fast energy ranges.

4.1. Nuclear data libraries used

The base case analysis used ENDF-8.0 nuclear data (Brown et al., 2018a) for all isotopes in the model. The ACE files were taken from the Lib80x library (Conlin et al., 2018). Additional results were generated by swapping in different nuclear data sources for ^{181}Ta only, while keeping the remaining nuclear data from ENDF-8.0. For the present work, the ENDF-8.0 ^{181}Ta RRR was extended to 2.544 keV and the URR minimum energy was changed from 330 eV to 2.544 keV, while the rest of the ENDF-8.0 nuclear data file was unchanged. In this way, reactivity effects due to changes in the ^{181}Ta cross section are emphasized. However, it is important to note that the reactivity of integral systems such as benchmark models, is dependent on the entire suite of nuclear data, and the elimination of an error in one cross section could possibly exacerbate errors in others. The ^{181}Ta ACE files for JEFF-3.3 (Plompen et al., 2020), JENDL-5.0 (Iwamoto et al., 2023) and the present work were generated using NJOY2016.70 (Macfarlane et al., 2017), Doppler broadened to 293.6 K, with probability tables generated for the URR.

4.2. Validation results

Results for PMM003, cases 1–5, are provided in Table 2, showing the published benchmark with uncertainty (1σ), the MCNP calculated with uncertainty (95% CI), the energy of average neutron lethargy causing fission (EALF) in units of MeV, and the value $C/E - 1$, where C represents the MCNP calculated k_{eff} and E represents the published benchmark k_{eff}.

Results are plotted in Fig. 20, showing the trends in $C/E - 1$ as a function of EALF. The $C/E - 1$ uncertainty for each nuclear data evaluation is less than the size of the symbols used in the figure. Lines

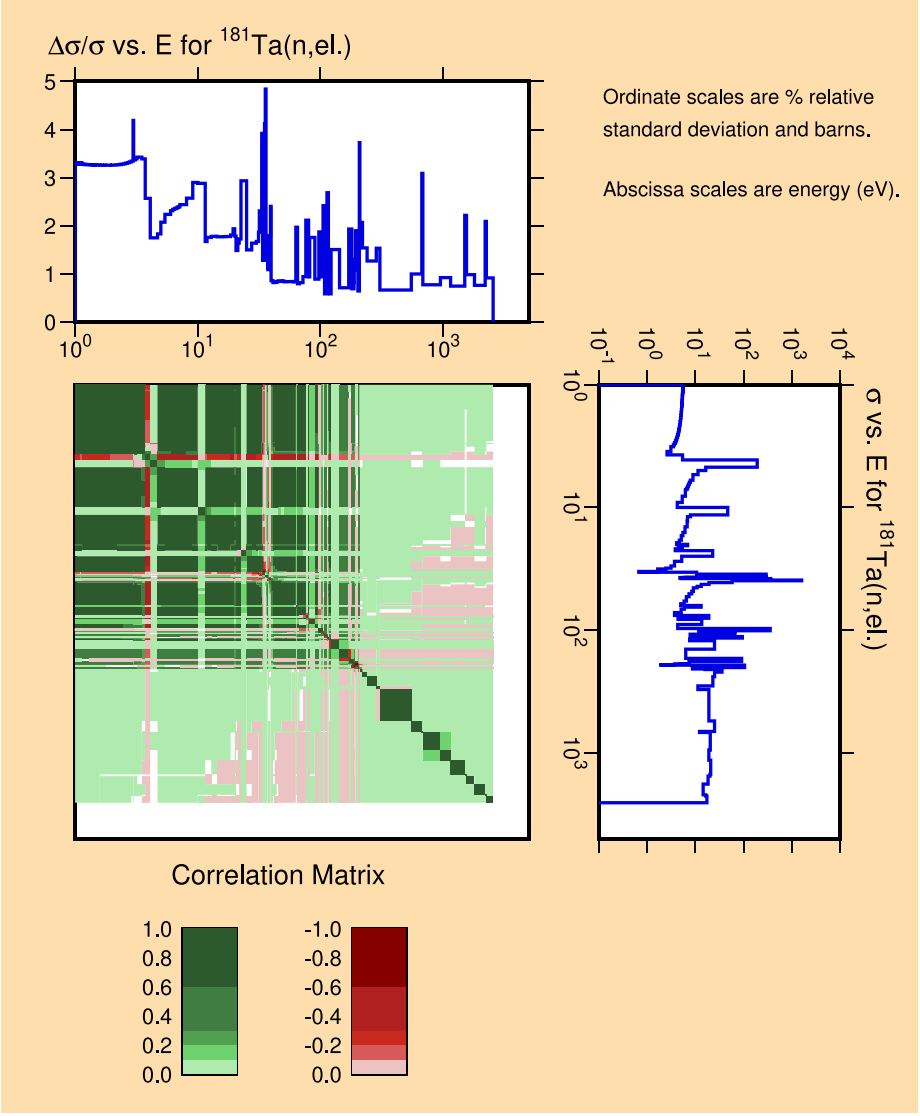

Fig. 18. The present ^{181}Ta elastic scattering cross section covariance. These data were generated using NJOY/ERRORR with a constant weighting flux. The energy bins were based on the SCALE 252-group structure (only using the energies bins below the RRR limit of 2.554 keV).

in between points are provided as an eye guide. Note the increasing bias in $C/E-1$ with increasing neutron spectrum hardness for all the data libraries, but most notably with JEFF-3.3 and JENDL-5.0. Using the ^{181}Ta evaluation from the present work serves to reduce the reactivity bias for cases 2–4, considerably. However, based on the high $C/E-1$ values for cases 1–3, there is still room for improvement. Given the neutron spectra associated with these cases, inclusion of a new fast region ^{181}Ta evaluation currently being performed (Herman, 2023) is hoped to improve agreement with experiments.

5. Conclusions

This work presents a new ^{181}Ta evaluation that extends the RRR energy region up to 2.554 keV and provides covariance information for all resonance parameters. The SAMMY R-matrix code was used to fit several high quality transmission and capture yield experimental data sets to obtain the present resonance parameters. A Monte Carlo approach was used to assign resonance spins, J, if not previously given in the neutron ATLAS-2018. The Monte Carlo approach was extended to add small fictitious resonances that improved the statistical distributions of RRR parameters.

The present RRR parameters resulted in a thermal capture resonance integral, RI_γ, that is ≈4% lower than ENDF-8.0, ≈7% higher than JEFF-3.3, ≈1% higher than JENDL-5.0, and ≈8% higher than the neutron ATLAS-2018. These differences are significantly influenced by the resonance parameters of the lowest energy resonance near 4.3 eV. In addition, the present RRR parameters generate thermal coherent and incoherent scattering values that agree within uncertainty to the values recommended by NIST.

The present RRR evaluation was validated using MCNP simulations of the plutonium Thermal/Epithermal Experiment (TEX-Pu) benchmark. The MCNP results show that the present ^{181}Ta RRR evaluation improves the reactivity bias for several benchmark cases. However, there is some room for improvement which may be provided with an updated fast region evaluation.

The present RRR evaluation has been submitted to the National Nuclear Data Center (NNDC) and are recommended for adoption into the next ^{181}Ta ENDF nuclear data library release.

Declaration of competing interest

The authors declare that they have no known competing financial interests or personal relationships that could have appeared to influence the work reported in this paper.

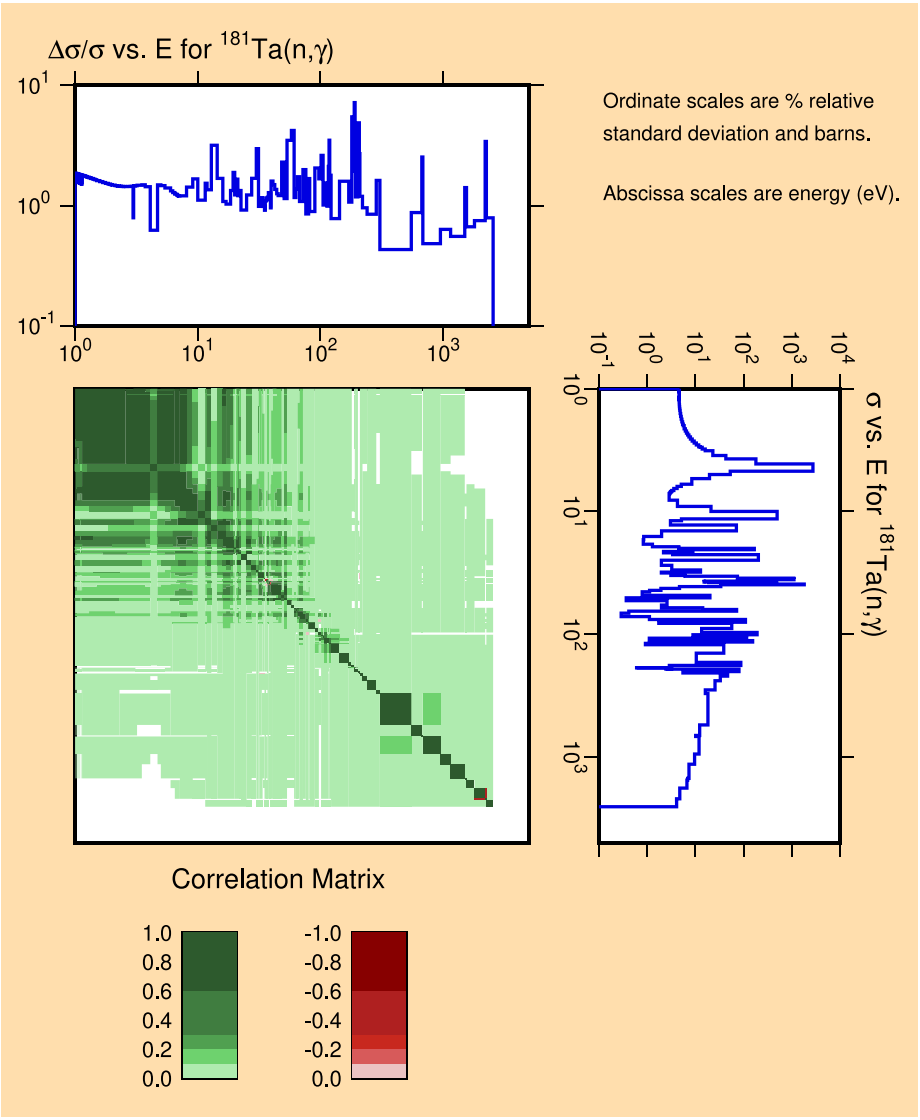

Fig. 19. The present ^{181}Ta radiative capture cross section covariance. These data were generated using NJOY/ERRORR with a constant weighting flux. The energy bins were based on the SCALE 252-group structure (only using the energies bins below the RRR limit of 2.554 keV).

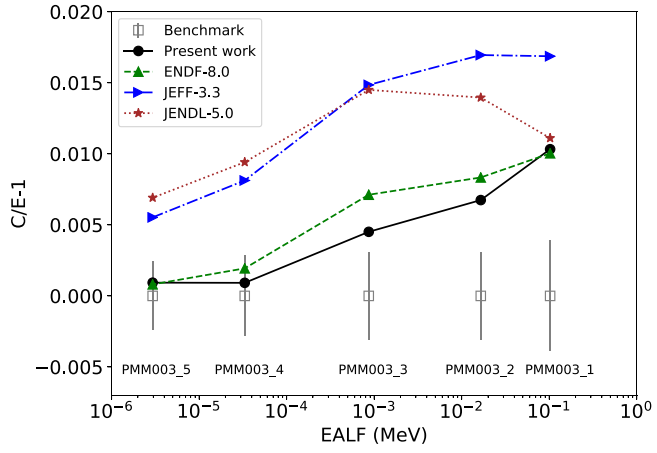

Fig. 20. Validation results for PMM003 showing increasing reactivity trends with increasing neutron spectrum hardness, and the improvement of the present work on C/E values for cases 2–4, which are most impacted by changes in the resolved resonance range. The C/E uncertainty for each nuclear data evaluation is less than the size of the symbol. Lines in between points are given as an eye guide.

Data availability

Data will be made available on request.

Acknowledgments

This manuscript has been authored by the Naval Nuclear Laboratory, operated by Fluor Marine Propulsion, LLC under Contract No. 89233018CNR000004 with the U.S. Department of Energy. The United States Government retains and the publisher, by accepting the article for publication, acknowledges that the United States Government retains a nonexclusive, paid-up, irrevocable, world-wide license to publish, distribute, translate, duplicate, exhibit, and perform the published form of this manuscript, or allow others to do so, for United States Government purposes. In addition, this work was supported by the US Department of Energy (DOE), Nuclear Criticality Safety Program (NCSP) funded and managed by the National Nuclear Security Administration (NNSA) for DOE, United States of America.

Appendix A. Resonance parameter values

See Table A.1.

Table A.1
The new ^{181}Ta resolved resonance region parameters presented in increasing energy order. All column names that start with a Δ symbol represent the uncertainty (1σ). The resonance energy, E, is given in units of eV, while the radiation width, Γ_γ, and neutron width, Γ_n, are given in units of meV. The resonance spin (i.e., total angular momentum) and the orbital angular momentum are represented by J and ℓ, respectively. All energies with an asterisk ($*$) represent a fictitious resonance (starting at 777.758 eV).

E (eV)	ΔE (eV)	Γ_γ (meV)	$\Delta\Gamma_\gamma$ (meV)	Γ_n (meV)	$\Delta\Gamma_n$ (meV)	J	ℓ
−7477.238	11.635	68.000	10.880	14475.800	2316.128	3.0	0
−7467.832	12.665	68.000	10.880	15763.500	2522.160	4.0	0
−19.050	0.071	25.500	4.080	63.000	10.080	4.0	0
−11.400	0.040	25.500	4.080	25.000	4.000	3.0	0
4.280	0.001	54.116	0.729	3.532	0.024	4.0	0
10.347	0.001	61.641	1.097	4.816	0.059	3.0	0
13.915	0.002	72.847	2.077	0.657	0.021	4.0	0
20.312	0.001	63.705	1.414	1.066	0.013	3.0	0
22.740	0.002	67.118	2.058	0.215	0.006	3.0	0
23.951	0.001	60.112	1.241	5.640	0.063	4.0	0
30.074	0.003	70.297	2.105	0.332	0.009	3.0	0
34.219	0.004	68.192	2.167	0.132	0.007	4.0	0
35.165	0.001	60.854	1.572	15.916	0.207	3.0	0
35.934	0.001	61.959	1.672	16.057	0.192	4.0	0
39.153	0.001	56.154	1.166	47.545	0.304	4.0	0
49.161	0.003	67.891	2.022	1.278	0.031	3.0	0
57.574	0.005	67.695	2.154	0.273	0.011	4.0	0
59.076	0.008	67.976	2.171	0.153	0.008	3.0	0
63.164	0.002	65.184	1.710	5.073	0.067	4.0	0
76.899	0.002	60.962	1.726	10.422	0.132	4.0	0
77.656	0.004	66.710	2.086	4.803	0.088	4.0	0
78.965	0.006	68.096	2.149	1.859	0.065	3.0	0
82.979	0.002	63.912	1.681	12.534	0.148	4.0	0
85.161	0.005	66.065	2.081	5.044	0.117	3.0	0
85.613	0.012	67.843	2.172	0.373	0.033	4.0	0
89.656	0.007	67.534	2.155	3.909	0.122	3.0	0
91.487	0.006	68.243	2.132	2.852	0.090	3.0	0
97.062	0.006	66.756	2.103	3.249	0.094	4.0	0
99.363	0.002	64.677	1.909	127.152	1.039	3.0	0
103.566	0.010	68.112	2.173	0.693	0.038	4.0	0
105.591	0.002	65.416	1.744	30.833	0.355	3.0	0
115.169	0.002	64.058	1.631	37.388	0.441	4.0	0
118.391	0.008	69.596	2.182	3.199	0.121	3.0	0
126.536	0.003	64.800	1.648	45.443	0.540	3.0	0
136.551	0.004	65.369	1.886	21.218	0.311	4.0	0
138.471	0.005	68.279	2.110	11.200	0.225	4.0	0
144.348	0.011	68.132	2.171	2.140	0.107	3.0	0
148.479	0.008	68.074	2.155	4.432	0.161	4.0	0
149.948	0.008	68.666	2.161	7.308	0.236	3.0	0
157.202	0.025	68.016	2.176	0.067	0.011	4.0	0
159.818	0.024	68.029	2.176	0.264	0.035	4.0	0
166.486	0.008	68.885	2.165	8.132	0.249	4.0	0
175.011	0.005	68.529	2.030	82.657	1.519	4.0	0
175.817	0.006	68.458	2.139	49.560	1.028	4.0	0
178.567	0.023	68.071	2.177	1.368	0.122	3.0	0
182.631	0.023	68.108	2.177	0.819	0.077	4.0	0
185.532	0.025	68.067	2.177	0.627	0.062	4.0	0
189.280	0.026	68.073	2.177	0.763	0.075	3.0	0
194.890	0.004	69.917	1.940	104.447	1.346	4.0	0
200.145	0.005	69.563	2.092	41.838	0.714	3.0	0
204.725	0.017	68.108	2.176	3.033	0.181	3.0	0
208.538	0.009	68.211	2.155	13.622	0.441	3.0	0
215.140	0.005	68.636	2.022	64.384	1.041	3.0	0
216.643	0.009	68.202	2.157	20.008	0.567	3.0	0
219.874	0.009	68.501	2.161	13.952	0.411	4.0	0
222.313	0.018	68.270	2.178	2.860	0.165	4.0	0
225.205	0.007	69.179	2.139	22.246	0.520	4.0	0
230.649	0.007	67.767	2.106	28.477	0.706	3.0	0
232.338	0.006	68.778	2.113	59.136	1.013	3.0	0
237.307	0.029	68.001	2.176	1.544	0.144	3.0	0
242.682	0.012	68.247	2.170	10.221	0.437	3.0	0
247.203	0.017	68.110	2.175	5.991	0.315	3.0	0
248.336	0.026	68.128	2.177	1.979	0.154	4.0	0
253.151	0.040	68.004	2.176	0.141	0.022	4.0	0
259.222	0.013	69.925	2.195	9.801	0.410	4.0	0
263.279	0.006	69.609	2.103	45.986	0.905	4.0	0

(*continued on next page*)

Table A.1 (*continued*).

E (eV)	ΔE (eV)	Γ_γ (meV)	$\Delta\Gamma_\gamma$ (meV)	Γ_n (meV)	$\Delta\Gamma_n$ (meV)	J	ℓ
264.697	0.014	68.470	2.178	10.626	0.455	4.0	0
271.832	0.014	68.595	2.177	9.854	0.421	4.0	0
273.812	0.006	69.059	2.087	108.988	1.738	3.0	0
277.310	0.009	67.896	2.138	27.821	0.725	4.0	0
280.362	0.011	69.206	2.179	20.788	0.717	3.0	0
287.710	0.010	68.837	2.147	25.430	0.825	3.0	0
290.375	0.016	68.536	2.178	14.444	0.667	4.0	0
291.259	0.020	68.271	2.177	14.085	0.736	3.0	0
304.154	0.018	68.308	2.178	4.955	0.255	4.0	0
306.254	0.010	68.992	2.159	28.189	0.885	3.0	0
311.729	0.015	68.841	2.183	14.982	0.673	3.0	0
313.224	0.008	69.044	2.124	56.617	1.178	4.0	0
322.912	0.019	68.322	2.179	5.781	0.304	4.0	0
328.164	0.029	68.296	2.180	5.241	0.353	3.0	0
329.419	0.010	69.673	2.139	54.964	1.431	3.0	0
341.515	0.023	68.133	2.177	4.904	0.288	4.0	0
344.571	0.012	68.307	2.154	29.806	1.075	3.0	0
346.802	0.014	68.565	2.176	16.830	0.689	4.0	0
349.204	0.012	68.593	2.167	26.841	0.898	4.0	0
354.275	0.011	69.243	2.170	30.900	0.980	4.0	0
357.410	0.032	68.097	2.177	4.194	0.309	3.0	0
370.318	0.011	69.185	2.137	35.838	1.088	4.0	0
378.458	0.024	68.553	2.182	9.555	0.550	4.0	0
379.442	0.032	68.211	2.179	5.766	0.403	4.0	0
382.011	0.060	67.994	2.176	0.242	0.037	4.0	0
388.964	0.015	68.421	2.161	25.460	1.041	3.0	0
396.679	0.028	68.132	2.175	10.939	0.734	4.0	0
397.677	0.016	68.287	2.154	36.729	1.486	3.0	0
410.043	0.009	66.846	1.984	82.553	1.828	4.0	0
416.184	0.017	67.867	2.133	83.168	3.798	3.0	0
416.952	0.022	67.439	2.141	62.542	3.500	3.0	0
419.947	0.060	68.011	2.176	1.084	0.143	4.0	0
421.905	0.049	68.025	2.176	2.676	0.273	3.0	0
429.068	0.025	68.058	2.175	6.662	0.385	4.0	0
434.341	0.015	68.297	2.155	30.780	1.220	3.0	0
439.366	0.013	70.136	2.157	61.873	1.963	3.0	0
443.495	0.031	68.535	2.179	27.557	2.455	3.0	0
444.176	0.023	68.382	2.164	55.275	3.139	3.0	0
446.266	0.012	68.383	2.149	69.099	2.054	3.0	0
449.770	0.025	68.057	2.175	10.138	0.555	4.0	0
461.594	0.013	67.588	2.090	43.471	1.492	4.0	0
465.219	0.032	68.097	2.177	7.053	0.453	3.0	0
467.764	0.011	66.259	2.042	87.228	2.166	4.0	0
471.648	0.014	67.883	2.146	37.296	1.357	4.0	0
473.479	0.050	68.007	2.176	1.911	0.265	4.0	0
482.422	0.027	68.406	2.177	18.408	1.036	3.0	0
483.727	0.034	68.124	2.177	8.523	0.576	4.0	0
490.314	0.016	67.175	2.128	34.548	1.369	4.0	0
494.085	0.033	68.116	2.176	11.139	0.693	3.0	0
495.455	0.035	68.064	2.176	7.430	0.479	4.0	0
497.668	0.074	67.985	2.176	0.874	0.117	4.0	0
500.161	0.053	68.066	2.177	3.053	0.289	4.0	0
502.099	0.013	67.681	2.112	58.242	1.879	4.0	0
519.446	0.023	68.001	2.170	14.281	0.735	4.0	0
522.920	0.013	65.972	2.005	86.664	2.566	4.0	0
524.657	0.039	67.972	2.175	10.236	0.735	3.0	0
527.622	0.012	67.462	2.098	88.780	2.393	4.0	0
534.035	0.016	68.014	2.132	74.514	2.617	3.0	0
536.376	0.028	68.133	2.176	13.935	0.781	4.0	0
542.690	0.018	68.280	2.152	50.227	2.030	3.0	0
549.133	0.026	67.948	2.170	17.261	0.934	3.0	0
554.368	0.049	68.038	2.176	4.899	0.400	4.0	0
556.577	0.072	68.046	2.177	5.679	0.843	3.0	0
557.205	0.022	68.630	2.162	39.014	1.877	4.0	0
561.260	0.078	67.991	2.176	1.893	0.246	3.0	0
567.209	0.061	68.019	2.176	3.282	0.328	4.0	0
569.642	0.018	67.547	2.100	62.146	2.463	3.0	0
576.326	0.056	68.066	2.177	5.628	0.470	3.0	0
588.642	0.089	67.996	2.176	0.700	0.103	4.0	0
591.713	0.017	65.803	2.071	37.819	1.628	4.0	0
596.156	0.052	67.661	2.166	35.366	3.685	4.0	0
596.782	0.013	67.017	2.105	470.300	8.096	3.0	0
606.259	0.049	68.088	2.177	7.682	0.577	4.0	0

(*continued on next page*)

Table A.1 (*continued*).

E (eV)	ΔE (eV)	Γ_γ (meV)	$\Delta\Gamma_\gamma$ (meV)	Γ_n (meV)	$\Delta\Gamma_n$ (meV)	J	ℓ
609.010	0.025	69.353	2.182	40.006	2.015	3.0	0
617.803	0.018	68.712	2.132	56.399	2.280	4.0	0
624.559	0.030	68.524	2.175	27.624	1.657	4.0	0
625.928	0.083	68.072	2.177	14.352	1.961	3.0	0
626.734	0.021	68.025	2.132	116.014	4.515	3.0	0
628.662	0.095	67.997	2.176	1.650	0.243	3.0	0
636.319	0.066	68.015	2.176	5.171	0.495	3.0	0
642.722	0.094	68.013	2.176	1.050	0.164	4.0	0
645.275	0.055	67.987	2.175	7.133	0.576	3.0	0
647.881	0.020	68.392	2.104	84.868	3.460	3.0	0
650.851	0.054	68.272	2.178	21.314	2.647	3.0	0
651.692	0.026	68.155	2.151	63.880	3.465	4.0	0
658.446	0.048	68.063	2.176	10.420	0.819	3.0	0
667.134	0.052	68.098	2.177	8.718	0.664	4.0	0
668.718	0.067	68.073	2.177	7.334	0.660	3.0	0
675.217	0.088	68.017	2.176	2.238	0.278	4.0	0
678.419	0.043	67.991	2.175	9.375	0.644	4.0	0
681.092	0.021	67.987	2.130	48.340	2.255	4.0	0
696.477	0.021	67.367	2.100	50.492	2.363	4.0	0
700.226	0.095	68.012	2.176	2.074	0.266	4.0	0
702.994	0.032	68.104	2.169	25.873	1.429	3.0	0
706.990	0.018	67.625	2.075	135.242	4.563	3.0	0
710.639	0.058	67.966	2.175	8.350	0.749	3.0	0
716.417	0.018	65.810	2.043	97.690	3.551	4.0	0
729.244	0.113	67.998	2.176	1.688	0.275	3.0	0
729.760	0.035	67.528	2.163	17.668	1.115	4.0	0
732.405	0.017	66.863	2.035	157.214	4.772	4.0	0
736.208	0.028	67.471	2.147	41.543	2.197	3.0	0
739.736	0.019	69.245	2.137	105.768	3.786	4.0	0
747.749	0.023	67.202	2.131	52.226	2.457	4.0	0
752.547	0.118	67.999	2.176	0.650	0.101	4.0	0
756.159	0.096	68.009	2.176	3.285	0.428	4.0	0
758.000	0.025	66.735	2.107	56.526	2.776	4.0	0
760.892	0.045	68.287	2.178	18.115	1.221	4.0	0
769.555	0.073	68.003	2.176	7.321	0.696	3.0	0
777.037	0.074	67.902	2.172	22.793	3.067	3.0	0
777.342	0.051	67.369	2.154	42.181	4.046	3.0	0
777.758*	0.123	68.005	2.176	1.370	0.221	4.0	0
782.787	0.116	68.001	2.176	1.948	0.264	3.0	0
789.642	0.027	69.074	2.147	68.872	3.467	3.0	0
798.076	0.030	68.575	2.167	42.845	2.261	3.0	0
801.162	0.126	67.997	2.176	0.803	0.124	3.0	0
802.469	0.128	68.000	2.176	0.137	0.022	4.0	0
805.593	0.092	67.959	2.175	3.647	0.407	4.0	0
807.408	0.129	68.000	2.176	0.089	0.014	4.0	0
808.753	0.022	66.819	2.104	56.142	2.477	4.0	0
813.563	0.019	65.864	2.040	109.033	3.941	4.0	0
816.063	0.125	67.996	2.176	1.889	0.276	3.0	0
817.131	0.122	67.999	2.176	2.122	0.299	3.0	0
821.408	0.020	67.391	2.095	143.460	5.133	3.0	0
825.941	0.042	67.989	2.174	16.512	1.038	4.0	0
830.987	0.097	68.007	2.176	2.474	0.328	4.0	0
833.833	0.025	67.748	2.148	51.736	2.350	4.0	0
846.280	0.064	68.202	2.177	20.468	1.745	3.0	0
847.571	0.054	67.822	2.169	18.622	1.505	4.0	0
853.088	0.028	67.505	2.139	53.759	2.704	3.0	0
855.541	0.135	68.001	2.176	0.639	0.102	4.0	0
862.045	0.137	68.001	2.176	0.379	0.060	4.0	0
870.293	0.098	68.099	2.177	9.458	1.215	3.0	0
871.253	0.056	68.205	2.177	15.792	1.347	4.0	0
874.616	0.026	67.618	2.132	48.455	2.327	4.0	0
879.523	0.032	67.821	2.152	56.626	2.908	3.0	0
881.522	0.044	67.902	2.173	12.974	1.060	4.0	0
887.069	0.120	68.006	2.176	3.332	0.413	4.0	0
888.924	0.068	68.051	2.176	12.195	0.964	3.0	0
895.411	0.032	68.115	2.152	44.419	2.217	4.0	0
897.611	0.037	68.073	2.170	29.488	1.645	4.0	0
907.181	0.115	67.992	2.176	4.308	0.497	4.0	0
909.112	0.029	66.641	2.114	61.377	3.075	4.0	0
910.485	0.125	67.966	2.175	4.783	0.725	3.0	0
913.438	0.025	68.602	2.130	120.008	5.339	3.0	0
915.956	0.035	67.921	2.159	49.133	2.557	3.0	0
919.905	0.030	67.677	2.155	42.528	2.128	4.0	0

(*continued on next page*)

Table A.1 (*continued*).

E (eV)	ΔE (eV)	Γ_γ (meV)	$\Delta\Gamma_\gamma$ (meV)	Γ_n (meV)	$\Delta\Gamma_n$ (meV)	J	ℓ
926.144	0.026	67.394	2.144	53.686	2.523	4.0	0
930.350	0.028	68.136	2.137	116.353	5.723	4.0	0
932.241	0.036	67.653	2.143	103.876	5.776	3.0	0
937.100	0.072	68.040	2.176	8.979	0.741	4.0	0
942.850	0.023	67.262	2.093	132.085	5.298	4.0	0
945.878	0.028	68.408	2.138	216.198	8.974	3.0	0
948.205	0.029	67.489	2.124	140.115	6.171	4.0	0
952.801	0.043	68.176	2.175	27.190	1.723	4.0	0
956.474	0.111	68.000	2.176	5.288	0.609	4.0	0
965.493	0.067	68.330	2.178	26.236	2.710	4.0	0
966.893	0.055	67.864	2.157	68.397	5.107	3.0	0
969.116	0.046	67.879	2.167	30.060	1.839	4.0	0
974.289	0.031	68.045	2.148	70.886	3.535	3.0	0
982.867	0.078	68.149	2.177	20.394	2.495	4.0	0
983.799	0.064	67.930	2.169	31.363	3.060	4.0	0
986.370	0.155	67.994	2.176	1.385	0.207	3.0	0
989.399	0.093	68.066	2.177	10.054	0.972	3.0	0
994.248	0.043	68.201	2.175	29.259	2.056	3.0	0
996.739	0.036	67.569	2.151	42.885	2.391	4.0	0
1002.392	0.033	68.237	2.152	70.075	3.571	3.0	0
1006.921	0.066	68.226	2.176	12.451	1.036	4.0	0
1016.441	0.034	68.400	2.169	47.953	2.802	3.0	0
1019.386	0.041	68.081	2.162	46.315	2.681	3.0	0
1026.256	0.067	67.966	2.174	12.358	0.962	4.0	0
1031.492	0.072	68.035	2.175	18.555	1.407	3.0	0
1033.897	0.052	67.871	2.163	38.077	2.500	4.0	0
1036.207	0.025	65.954	2.062	276.120	8.635	4.0	0
1043.868	0.033	67.680	2.160	85.917	9.045	3.0	0
1043.914	0.032	67.686	2.157	92.577	9.160	3.0	0
1056.431	0.043	67.963	2.164	41.145	2.339	3.0	0
1064.231	0.037	68.951	2.160	65.776	3.505	3.0	0
1071.881	0.031	70.217	2.152	164.436	7.748	4.0	0
1073.913	0.057	67.477	2.154	41.474	3.109	4.0	0
1078.787	0.107	68.138	2.178	15.701	1.698	3.0	0
1080.779	0.048	67.857	2.149	75.939	4.681	4.0	0
1082.696	0.054	67.736	2.161	45.775	3.417	4.0	0
1091.250	0.030	67.463	2.124	158.970	7.297	3.0	0
1094.344	0.061	68.322	2.176	38.827	2.673	3.0	0
1097.556	0.035	67.864	2.146	83.473	4.298	4.0	0
1103.927	0.134	68.027	2.176	6.037	0.709	4.0	0
1105.776	0.175	68.002	2.176	1.251	0.198	3.0	0
1113.379	0.039	69.033	2.179	55.959	3.576	3.0	0
1119.947	0.047	67.980	2.175	9.609	1.053	4.0	0
1131.499	0.051	68.809	2.158	77.200	7.454	4.0	0
1132.581	0.069	67.451	2.142	86.017	8.984	3.0	0
1138.925	0.085	68.153	2.177	14.287	1.167	4.0	0
1145.857	0.033	69.428	2.155	123.409	5.863	3.0	0
1151.926	0.029	67.691	2.095	165.132	6.660	4.0	0
1157.703	0.042	67.353	2.147	46.408	2.678	4.0	0
1165.885	0.036	68.101	2.137	100.272	5.137	3.0	0
1175.709	0.034	68.883	2.140	135.680	6.753	4.0	0
1176.200*	0.185	68.002	2.176	5.366	0.844	3.0	0
1178.748	0.036	68.425	2.127	199.300	9.187	4.0	0
1180.448	0.101	67.888	2.172	29.577	3.599	3.0	0
1192.395	0.025	68.020	2.138	779.252	16.297	3.0	0
1194.242*	0.181	67.990	2.176	6.856	1.136	3.0	0
1204.524	0.026	68.217	2.175	24.676	2.163	4.0	0
1209.160	0.080	68.052	2.172	27.264	2.202	3.0	0
1212.570	0.027	68.285	2.178	25.484	2.538	3.0	0
1216.693	0.182	67.993	2.176	2.820	0.408	4.0	0
1219.292	0.077	67.520	2.165	23.529	2.050	4.0	0
1221.076	0.108	67.856	2.173	13.897	1.384	4.0	0
1227.541	0.039	68.831	2.152	110.314	5.866	3.0	0
1233.404	0.146	68.006	2.176	8.156	0.971	3.0	0
1238.247	0.193	68.003	2.176	1.561	0.252	4.0	0
1240.561	0.066	67.994	2.174	15.967	1.491	4.0	0
1246.946	0.067	67.625	2.150	72.294	6.478	3.0	0
1248.588	0.060	66.534	2.123	75.342	6.035	4.0	0
1252.121	0.195	67.998	2.176	1.938	0.310	3.0	0
1259.992	0.044	67.756	2.145	90.621	5.251	3.0	0
1263.850	0.059	68.022	2.167	37.427	2.504	4.0	0
1268.750	0.036	67.991	2.176	7.122	0.864	4.0	0
1272.356*	0.202	68.000	2.176	0.939	0.150	3.0	0

(*continued on next page*)

Table A.1 (*continued*).

E (eV)	ΔE (eV)	Γ_γ (meV)	$\Delta\Gamma_\gamma$ (meV)	Γ_n (meV)	$\Delta\Gamma_n$ (meV)	J	ℓ
1276.594	0.039	66.302	2.102	83.264	4.432	4.0	0
1280.761	0.124	67.997	2.176	4.881	0.649	4.0	0
1283.991	0.027	68.240	2.178	19.104	1.749	4.0	0
1287.797	0.059	68.029	2.175	17.919	1.627	4.0	0
1292.098	0.133	68.237	2.179	20.449	2.088	3.0	0
1293.982	0.050	67.395	2.132	90.375	5.370	3.0	0
1300.616	0.033	69.055	2.139	163.827	7.214	4.0	0
1307.864	0.085	67.925	2.171	13.591	1.544	3.0	0
1311.126	0.195	68.005	2.176	3.342	0.485	4.0	0
1313.549	0.044	68.159	2.152	89.896	5.227	3.0	0
1317.901	0.047	67.521	2.136	85.009	4.858	3.0	0
1324.003	0.079	67.966	2.174	9.415	1.142	4.0	0
1328.552	0.163	68.095	2.177	21.844	3.089	3.0	0
1329.643	0.050	68.697	2.158	172.986	10.032	3.0	0
1332.932	0.051	68.209	2.157	199.986	12.797	3.0	0
1333.487	0.058	67.961	2.175	25.388	3.801	4.0	0
1336.013	0.056	66.597	2.129	74.424	5.272	4.0	0
1342.988	0.175	68.034	2.176	6.001	0.734	4.0	0
1350.193	0.199	67.998	2.176	3.352	0.502	4.0	0
1352.789	0.108	67.966	2.175	11.512	1.168	4.0	0
1360.140	0.199	67.997	2.176	4.728	0.761	4.0	0
1361.358	0.058	67.643	2.159	60.386	5.505	4.0	0
1362.930	0.104	66.985	2.140	90.414	8.801	4.0	0
1363.178	0.218	67.995	2.176	2.840	0.461	3.0	0
1364.464	0.070	65.519	2.100	108.149	9.652	4.0	0
1372.687	0.097	68.016	2.174	19.240	1.587	4.0	0
1377.704	0.060	68.031	2.155	73.813	5.502	4.0	0
1378.861	0.132	67.922	2.174	19.392	2.730	3.0	0
1388.895	0.026	68.544	2.179	47.883	4.016	3.0	0
1392.206	0.042	67.542	2.126	167.777	8.474	3.0	0
1399.088	0.039	68.224	2.115	184.272	8.835	4.0	0
1410.216	0.027	68.042	2.176	17.196	2.016	3.0	0
1416.782*	0.224	68.001	2.176	1.833	0.298	3.0	0
1418.181	0.095	67.971	2.175	11.872	1.313	4.0	0
1427.399	0.057	68.068	2.176	18.149	2.059	3.0	0
1431.725	0.048	68.752	2.144	133.305	7.531	3.0	0
1438.088	0.227	68.001	2.176	1.857	0.291	3.0	0
1441.328	0.209	68.005	2.176	5.352	0.748	3.0	0
1444.504	0.055	67.945	2.174	15.240	1.767	4.0	0
1451.543	0.064	68.453	2.165	55.423	3.916	4.0	0
1456.099	0.014	67.979	2.175	18.777	2.160	3.0	0
1464.194	0.230	68.002	2.176	2.708	0.408	3.0	0
1465.978	0.170	68.075	2.177	10.527	1.188	4.0	0
1469.246	0.085	68.150	2.178	14.761	1.645	4.0	0
1471.406	0.207	68.009	2.176	4.740	0.668	4.0	0
1473.961	0.234	68.000	2.176	1.721	0.273	3.0	0
1476.201	0.046	66.526	2.084	124.753	7.068	4.0	0
1487.795	0.222	67.999	2.176	4.272	0.660	3.0	0
1490.855	0.194	67.996	2.176	6.227	0.857	4.0	0
1494.786	0.229	68.002	2.176	2.287	0.355	4.0	0
1502.611	0.040	68.686	2.171	64.474	4.940	3.0	0
1503.163	0.240	67.999	2.176	0.803	0.128	3.0	0
1504.747	0.238	68.001	2.176	1.685	0.274	3.0	0
1508.355	0.211	68.029	2.176	4.382	0.655	4.0	0
1518.463	0.065	68.475	2.147	158.558	12.152	3.0	0
1520.685	0.089	67.386	2.139	83.841	7.358	4.0	0
1523.897	0.051	66.379	2.082	268.224	13.504	4.0	0
1525.549	0.161	67.786	2.172	21.901	3.211	3.0	0
1532.554	0.061	68.317	2.164	62.960	4.317	4.0	0
1537.851	0.151	67.998	2.176	12.038	1.426	4.0	0
1541.668	0.126	68.089	2.177	17.067	1.935	3.0	0
1555.512	0.095	68.250	2.172	47.281	6.264	4.0	0
1556.655	0.072	66.371	2.122	205.017	15.257	3.0	0
1566.114	0.050	65.840	2.084	110.721	6.878	4.0	0
1571.672	0.235	67.994	2.176	4.466	0.673	3.0	0
1577.251	0.199	67.994	2.176	8.807	1.150	4.0	0
1579.975	0.080	67.355	2.157	42.124	3.127	4.0	0
1586.132	0.078	67.247	2.136	98.482	8.694	4.0	0
1587.132	0.131	67.574	2.163	41.805	5.447	4.0	0
1592.020	0.034	68.072	2.172	42.483	4.032	3.0	0
1602.839	0.232	67.935	2.175	7.954	1.356	4.0	0
1603.631	0.063	66.048	2.109	145.353	9.677	3.0	0

(*continued on next page*)

Table A.1 (*continued*).

E (eV)	ΔE (eV)	Γ_γ (meV)	$\Delta\Gamma_\gamma$ (meV)	Γ_n (meV)	$\Delta\Gamma_n$ (meV)	J	ℓ
1608.719	0.055	66.483	2.125	83.289	5.665	4.0	0
1609.286*	0.252	67.979	2.176	4.602	0.764	3.0	0
1615.214	0.180	68.096	2.177	14.913	1.907	4.0	0
1617.429	0.068	67.069	2.131	92.039	6.463	4.0	0
1617.918*	0.256	67.990	2.176	4.311	0.701	3.0	0
1623.903	0.065	68.423	2.174	56.072	5.014	4.0	0
1625.776	0.116	68.153	2.174	42.237	4.131	4.0	0
1630.744	0.100	67.936	2.175	13.953	1.811	4.0	0
1631.178*	0.242	67.987	2.176	6.836	1.071	3.0	0
1637.803	0.153	68.018	2.176	16.921	1.855	3.0	0
1649.405	0.063	67.461	2.144	105.513	7.134	4.0	0
1650.805	0.156	67.982	2.176	15.168	2.340	3.0	0
1652.973	0.118	68.038	2.170	44.938	3.897	4.0	0
1655.800	0.115	67.876	2.162	98.035	9.572	3.0	0
1656.814	0.107	67.594	2.163	46.509	5.478	4.0	0
1671.474	0.070	68.093	2.164	83.096	5.666	3.0	0
1674.378	0.088	68.657	2.173	87.216	6.407	3.0	0
1679.045	0.061	68.335	2.150	138.723	8.716	4.0	0
1681.853	0.223	68.021	2.176	10.488	1.436	4.0	0
1684.523*	0.270	68.000	2.176	0.104	0.017	3.0	0
1693.261	0.089	67.850	2.165	48.557	3.938	4.0	0
1697.896	0.053	67.338	2.122	329.478	17.842	4.0	0
1699.885	0.133	67.880	2.170	55.062	7.303	3.0	0
1701.241	0.191	67.987	2.176	6.853	1.086	4.0	0
1705.004	0.201	68.017	2.176	12.535	1.631	4.0	0
1710.612*	0.267	67.999	2.176	3.150	0.510	3.0	0
1714.098	0.103	68.016	2.161	55.671	4.985	3.0	0
1720.998	0.071	67.722	2.150	74.351	5.033	4.0	0
1728.952	0.267	67.998	2.176	3.812	0.600	3.0	0
1733.624	0.097	68.451	2.167	146.081	16.114	3.0	0
1735.316	0.141	67.835	2.154	206.945	20.244	3.0	0
1736.933	0.099	66.744	2.129	205.617	19.313	3.0	0
1742.906	0.088	67.825	2.155	124.374	11.978	3.0	0
1743.843	0.042	67.828	2.168	45.395	5.681	4.0	0
1752.116	0.071	68.488	2.162	138.972	9.150	3.0	0
1767.838	0.142	68.475	2.179	48.500	4.663	3.0	0
1771.017	0.131	68.022	2.172	35.000	3.359	4.0	0
1776.002	0.282	67.998	2.176	1.876	0.303	3.0	0
1778.800*	0.263	67.980	2.176	4.301	0.760	4.0	0
1780.402*	0.270	67.986	2.176	3.671	0.633	4.0	0
1785.196	0.188	68.079	2.177	16.441	1.906	4.0	0
1793.430	0.186	68.010	2.175	23.331	2.640	3.0	0
1797.138	0.237	68.001	2.176	9.149	1.272	4.0	0
1801.778	0.076	67.067	2.127	88.389	5.993	4.0	0
1810.507	0.281	68.006	2.176	4.402	0.700	3.0	0
1811.231	0.030	68.070	2.177	19.762	2.498	4.0	0
1821.899*	0.290	67.999	2.176	1.178	0.187	4.0	0
1822.389	0.244	68.006	2.176	10.983	1.524	3.0	0
1830.493	0.051	67.997	2.176	9.367	1.323	4.0	0
1839.326	0.207	68.140	2.177	20.974	2.502	3.0	0
1843.478	0.166	68.282	2.177	36.296	4.360	4.0	0
1844.401*	0.283	68.016	2.176	9.053	1.415	3.0	0
1845.189	0.071	68.082	2.176	25.319	3.237	4.0	0
1848.282	0.109	67.977	2.176	8.037	1.235	4.0	0
1854.109*	0.210	67.987	2.176	7.920	1.294	3.0	0
1854.609	0.094	66.847	2.145	85.947	8.636	3.0	0
1854.996	0.285	67.957	2.175	8.052	1.333	3.0	0
1856.010	0.208	67.750	2.171	17.506	2.677	4.0	0
1866.395	0.075	67.918	2.149	94.511	6.581	4.0	0
1877.184	0.070	68.326	2.149	176.632	10.966	3.0	0
1887.654	0.074	67.108	2.126	117.771	8.338	4.0	0
1891.336	0.160	67.499	2.165	28.439	4.272	4.0	0
1893.098	0.110	67.075	2.155	54.758	6.833	3.0	0
1903.044	0.114	68.126	2.174	31.610	3.329	4.0	0
1909.872*	0.306	68.000	2.176	0.0005	0.00005	4.0	0
1910.649	0.258	68.006	2.176	10.519	1.499	3.0	0
1917.116	0.306	67.999	2.176	1.373	0.223	3.0	0
1917.519*	0.204	67.960	2.175	8.004	1.246	4.0	0
1927.059*	0.307	67.999	2.176	1.161	0.186	4.0	0
1929.573	0.056	67.414	2.148	82.666	7.897	3.0	0
1934.371	0.092	66.784	2.130	84.550	6.994	4.0	0
1937.136	0.084	67.926	2.175	12.883	1.841	4.0	0

(*continued on next page*)

Table A.1 (*continued*).

E (eV)	ΔE (eV)	Γ_γ (meV)	$\Delta\Gamma_\gamma$ (meV)	Γ_n (meV)	$\Delta\Gamma_n$ (meV)	J	ℓ
1937.619*	0.307	67.995	2.176	2.986	0.475	3.0	0
1941.938	0.181	67.827	2.171	33.862	3.860	3.0	0
1943.629	0.288	67.976	2.176	7.433	1.171	4.0	0
1945.365	0.028	67.901	2.171	36.155	4.294	4.0	0
1951.088	0.086	68.391	2.161	96.137	7.309	4.0	0
1959.949	0.184	68.084	2.177	17.721	2.236	3.0	0
1965.482	0.047	67.866	2.171	31.991	3.472	4.0	0
1969.125*	0.315	68.000	2.176	0.027	0.004	3.0	0
1970.296	0.293	68.009	2.176	6.748	0.996	4.0	0
1971.681	0.056	68.029	2.176	26.060	2.981	4.0	0
1979.054*	0.310	67.997	2.176	3.504	0.574	3.0	0
1981.812*	0.304	67.996	2.176	5.391	0.904	3.0	0
1982.903	0.269	67.983	2.176	7.657	1.234	4.0	0
1990.215	0.169	68.061	2.176	22.633	2.667	4.0	0
1997.708	0.058	67.898	2.173	23.291	3.320	4.0	0
1999.445	0.141	67.969	2.164	93.070	8.391	3.0	0
2001.840	0.203	67.698	2.169	24.437	3.420	4.0	0
2001.908*	0.310	67.955	2.175	9.965	1.635	3.0	0
2005.573	0.208	67.925	2.174	17.459	2.167	4.0	0
2015.414	0.130	68.977	2.180	140.126	14.683	3.0	0
2016.964	0.235	68.475	2.178	92.686	12.165	3.0	0
2018.924	0.195	68.503	2.176	118.377	12.913	3.0	0
2021.161	0.155	68.352	2.172	123.589	12.067	3.0	0
2024.230	0.091	67.597	2.163	55.828	6.233	4.0	0
2033.505	0.314	68.010	2.176	5.107	0.773	3.0	0
2038.636	0.047	68.379	2.178	81.276	9.140	3.0	0
2038.927	0.169	68.103	2.177	27.183	3.606	4.0	0
2057.140	0.049	68.378	2.176	50.592	5.454	4.0	0
2063.316	0.025	68.044	2.162	71.201	7.069	4.0	0
2069.648	0.018	68.040	2.176	16.454	2.301	4.0	0
2071.423	0.091	67.993	2.176	10.897	1.635	3.0	0
2084.929*	0.334	68.000	2.176	0.0001	0.00001	3.0	0
2084.956	0.258	67.992	2.176	15.398	2.213	4.0	0
2087.956	0.094	66.926	2.125	162.577	12.079	4.0	0
2089.677	0.247	67.811	2.172	26.901	4.165	3.0	0
2092.621	0.332	67.999	2.176	4.018	0.645	3.0	0
2095.304	0.188	67.991	2.173	31.780	3.525	4.0	0
2099.296	0.024	68.061	2.176	29.327	3.701	3.0	0
2109.868	0.031	68.015	2.172	45.047	5.153	3.0	0
2113.894	0.332	67.998	2.176	2.802	0.431	4.0	0
2120.723*	0.307	67.999	2.176	5.440	0.861	4.0	0
2123.848	0.113	67.663	2.156	65.882	5.991	4.0	0
2132.818	0.107	68.725	2.168	201.519	19.524	3.0	0
2134.753	0.110	67.744	2.151	111.962	10.497	4.0	0
2140.281*	0.341	68.001	2.176	1.047	0.168	4.0	0
2148.536	0.042	68.329	2.168	105.904	9.989	3.0	0
2152.679	0.083	68.330	2.158	302.786	20.042	4.0	0
2153.470*	0.335	67.997	2.176	12.970	2.048	3.0	0
2154.133	0.028	67.885	2.172	50.865	6.817	4.0	0
2157.525*	0.300	67.981	2.176	10.598	1.641	3.0	0
2167.034	0.158	67.756	2.166	49.173	5.070	4.0	0
2169.514	0.070	67.567	2.163	82.001	8.246	3.0	0
2172.200*	0.348	68.000	2.176	0.067	0.011	4.0	0
2173.747*	0.348	68.000	2.176	0.366	0.059	3.0	0
2179.697*	0.349	68.000	2.176	0.148	0.024	3.0	0
2186.996	0.035	68.037	2.161	78.506	7.825	4.0	0
2192.361	0.157	68.777	2.177	93.374	10.909	4.0	0
2194.955	0.090	68.391	2.146	402.267	25.428	4.0	0
2199.797	0.193	67.951	2.169	58.489	6.471	3.0	0
2207.902*	0.352	68.001	2.176	1.872	0.299	4.0	0
2210.770	0.093	67.329	2.138	196.320	13.758	3.0	0
2220.310	0.051	67.886	2.166	59.766	6.314	4.0	0
2222.474*	0.356	68.000	2.176	0.005	0.001	3.0	0
2225.503	0.319	67.989	2.176	7.688	1.182	4.0	0
2236.128	0.085	68.817	2.178	102.258	10.700	3.0	0
2239.526	0.165	68.232	2.168	75.429	7.767	4.0	0
2242.164	0.145	67.509	2.155	111.173	10.391	3.0	0
2246.130*	0.353	67.999	2.176	3.622	0.570	4.0	0
2251.905*	0.320	68.078	2.177	13.612	2.031	3.0	0
2255.139	0.225	68.270	2.180	24.339	2.861	4.0	0
2262.353*	0.243	67.988	2.174	28.351	3.731	3.0	0
2262.297	0.359	68.001	2.176	2.744	0.437	4.0	0
2269.896*	0.352	68.007	2.176	7.345	1.127	3.0	0

(*continued on next page*)

Table A.1 (*continued*).

E (eV)	ΔE (eV)	Γ_γ (meV)	$\Delta\Gamma_\gamma$ (meV)	Γ_n (meV)	$\Delta\Gamma_n$ (meV)	J	ℓ
2270.054	0.302	68.029	2.176	13.422	1.847	4.0	0
2274.020	0.317	68.034	2.176	9.571	1.324	4.0	0
2280.522	0.055	68.614	2.179	75.097	8.271	3.0	0
2283.332	0.043	68.486	2.171	111.072	10.941	3.0	0
2291.419	0.110	67.965	2.168	68.221	7.541	4.0	0
2293.908	0.118	66.736	2.129	125.657	11.829	4.0	0
2294.626*	0.367	68.000	2.176	0.015	0.002	3.0	0
2299.819	0.040	68.103	2.176	29.335	3.541	4.0	0
2308.140	0.102	68.465	2.175	77.319	7.149	3.0	0
2310.910*	0.370	68.000	2.176	0.513	0.082	4.0	0
2322.355	0.147	68.383	2.174	130.827	18.009	3.0	0
2322.741*	0.371	68.002	2.176	3.650	0.577	4.0	0
2324.306	0.104	67.989	2.156	684.671	41.950	3.0	0
2329.070	0.132	67.615	2.145	145.641	13.089	4.0	0
2335.543	0.168	68.612	2.176	95.212	8.665	3.0	0
2338.957*	0.374	68.000	2.176	1.202	0.190	4.0	0
2345.571	0.130	68.887	2.172	137.531	11.157	4.0	0
2348.698	0.061	68.204	2.170	107.733	12.232	3.0	0
2350.953	0.315	68.007	2.176	19.372	2.625	4.0	0
2357.722	0.163	68.384	2.177	62.626	6.305	3.0	0
2361.791*	0.139	68.007	2.176	10.038	1.549	3.0	0
2366.504	0.030	68.260	2.175	57.088	6.488	4.0	0
2370.841	0.219	68.016	2.174	37.750	4.337	4.0	0
2376.726	0.104	67.711	2.166	61.121	6.747	3.0	0
2380.787*	0.221	67.948	2.175	7.682	1.352	4.0	0
2384.590*	0.359	67.991	2.176	3.533	0.587	4.0	0
2385.572*	0.377	67.997	2.176	2.507	0.413	4.0	0
2386.422*	0.094	67.994	2.176	5.126	0.847	3.0	0
2392.007	0.113	68.346	2.159	192.369	15.705	4.0	0
2394.059	0.038	68.144	2.175	56.607	7.344	4.0	0
2402.096	0.084	69.539	2.181	509.485	28.304	3.0	0
2407.688	0.122	68.125	2.176	34.597	4.434	4.0	0
2412.442*	0.366	68.016	2.176	8.779	1.341	3.0	0
2418.506	0.324	68.013	2.176	14.604	2.059	4.0	0
2418.620*	0.387	68.000	2.176	0.026	0.004	3.0	0
2432.744	0.273	68.094	2.177	20.178	2.608	4.0	0
2433.073*	0.389	68.000	2.176	0.096	0.015	3.0	0
2441.315	0.351	68.039	2.177	13.720	1.944	3.0	0
2443.064*	0.388	68.000	2.176	2.024	0.320	4.0	0
2453.412	0.142	68.834	2.169	155.824	12.558	3.0	0
2453.453*	0.393	68.000	2.176	0.100	0.016	4.0	0
2456.675*	0.372	68.027	2.176	12.524	1.864	3.0	0
2459.552	0.165	68.360	2.168	90.311	9.318	4.0	0
2463.756*	0.393	68.000	2.176	1.895	0.306	3.0	0
2472.475	0.386	68.005	2.176	4.726	0.750	4.0	0
2478.626	0.073	68.312	2.177	64.927	8.575	4.0	0
2479.959	0.298	68.095	2.176	58.590	7.821	3.0	0
2486.870	0.096	68.116	2.170	93.153	10.499	3.0	0
2488.072*	0.375	68.018	2.176	11.860	1.759	4.0	0
2496.213	0.149	68.174	2.165	166.483	14.432	3.0	0
2497.502*	0.153	67.992	2.176	11.158	1.749	4.0	0
2501.153*	0.396	68.002	2.176	4.335	0.691	3.0	0
2502.857	0.294	68.099	2.177	19.393	2.685	4.0	0
2513.009	0.255	67.919	2.173	28.675	3.642	4.0	0
2518.095*	0.403	68.000	2.176	1.269	0.202	3.0	0
2521.496	0.107	69.055	2.165	240.192	16.899	4.0	0
2526.511	0.135	67.909	2.162	129.815	13.103	3.0	0
2526.766*	0.404	68.000	2.176	1.326	0.212	4.0	0
2532.936	0.243	68.087	2.173	63.924	7.623	3.0	0
2534.670*	0.367	67.997	2.176	11.310	1.785	4.0	0
2546.905	0.021	68.166	2.174	50.612	5.963	4.0	0
9967.942	14.468	68.000	10.880	15612.000	2497.920	4.0	0
9988.877	16.596	68.000	10.880	18269.100	2923.056	3.0	0

References

Baum, E., Ernesti, M., Knox, H., Miller, T., Watson, A., Nuclides and Isotopes: Chart of the Nuclides, seventeenth ed. Knolls Atomic Power Laboratory, Bechtel Marine Propulsion Corporation (2010).

Bess, J.D., Ivanova, T., Martin, J., Hill, I., Scott, L., 2020. The 2020 edition of the ICSBEP handbook. Nuclear Energy Agency, Organiz. Econ. Co-Oper. Development.

Brown, J.M., 2019. Measurements, Evaluation, and Validation of Ta-181 Resolved and Unresolved Resonance Regions. Thesis, Rensselaer Polytechnic Institute.

Brown, J.M., Barry, D.P., Lewis, A., Trumbull, T., Pigni, M., Block, R.C., Danon, Y., 2024. New unresolved resonance parameter evaluation for ^{181}Ta with full covariance. Ann. Nucl. Energy (submitted for publication).

Brown, D.A., Chadwick, M.B., Capote, R., et al., 2018a. ENDF/B-VIII.0: the 8th major release of the nuclear reaction data library with CIELO-project cross sections, new standards and thermal scattering data. Nucl. Data Sheets 148, 1–142.

Brown, J.M., Leinweber, G., Barry, D.P., Epping, B., Rapp, M., Danon, Y., 2018b. Improved transmission and capture data for Tantalum-181. ANS Trans. 118, 21–24.

Chambers, A., 2022. Five-Year Execution Plan for the Mission and Vision of the United States Department of Energy Nuclear Criticality Safety Program, FY 2023 through FY 2027, Revision 2. Tech. rep, US Department of Energy.

Conlin, J.L., Haeck, W., Neudecker, D., Parsons, D.K., White, M.C., 2018. Release of ENDF/B-VIII. 0-based ACE data files. Los Alamos National Laboratory, Los Alamos, NM, USA, Tech. Rep. la-UR-18-24034.

Danon, Y., Block, R., Slovacek, R., 1995. Design and construction of a thermal neutron target for the RPI LINAC. Nucl. Instrum. Methods Phys. Res. A 352 (3), 596–604.

Farina Arboccò, F., Vermaercke, P., Smits, K., Sneyers, L., Strijckmans, K., 2014. Experimental determination of k_0, Q_0 factors, effective resonance energies and neutron cross-sections for 37 isotopes of interest in NAA. J. Radioanal. Nucl. Chem. 302 (1), 655–672, EXFOR#23260137 (Accessed on 18 October 2022).

Fröhner, F.H., Bouland, O., 2001. Treatment of external levels in neutron resonance fitting: Application to the nonfissile nuclide ^{52}Cr. Nucl. Sci. Eng. 137 (1), 70–88.

Harvey, J., Hill, N., Perey, F., Tweed, G., Leal, L., 1988. High-resolution neutron transmission measurements on ^{235}U, ^{239}Pu, and ^{238}U. In: Conference on Nuclear Data for Science and Technology. Mito, Japan, pp. 115–118, EXFOR#13632012, EXFOR#13632013.

Heft, R., Mayaguez, 1978. A consistent set of nuclear-parameter values for absolute INAA. In: Conference on Computers in Activation Analysis and Gamma-Ray Spectroscopy. p. 495, EXFOR#12866180 (Accessed on 18 October 2022).

Herman, M., 2023. Los alamos national laboratory, private communication.

Herman, M., Trkov, A., 2010. ENDF-6 Formats Manual. Tech. Rep BNL-90365-2009, Brookhaven National Laboratory.

Ho, C.Y., Powell, R.W., Liley, P.E., 1974. Thermal conductivity of the elements: A comprehensive review. J. Phys. Chem. Ref. Data 3 (1), 1–796.

Iwamoto, O., Iwamoto, N., Kunieda, S., Minato, F., Nakayama, S., Abe, Y., Tsubakihara, K., Okumura, S., Ishizuka, C., Yoshida, T., et al., 2023. Japanese evaluated nuclear data library version 5: JENDL-5. J. Nucl. Sci. Technol. 60 (1), 1–60.

Jani, A., 1985. Phonon Density of States and Debye Temperatures of BCC Transition Metals. Z. Naturforschung A 40 (8), 834–842.

Koester, L., Knopf, K., 1971. Measurements of neutron-scattering-amplitudes using the christiansen filter technique. Z. Nat.forsch. A 26 (3), 391–399, EXFOR#20758008 (Accessed on Dec. 1, 2021).

Koester, L., Rauch, H., Seymann, E., 1991. Neutron scattering lengths: A survey of experimental data and methods. At. Data Nucl. Data Tables 49 (1), 65–120.

Lamb, Jr., W.E., 1939. Capture of neutrons by atoms in a crystal. Phys. Rev. 55 (2), 190.

Larson, N., 2008. Updated Users' Guide for SAMMY. Tech. Rep. ORNL/TM-9179/R8, Oak Ridge National Laboratory.

Macfarlane, R., Muir, D.W., Boicourt, R.M., Kahler, III, A.C., Conlin, J.L., 2017. The NJOY nuclear data processing system, version 2016.

Malik, S., Brunhart, G., Shore, F., Sailor, V., 1970. Factors in the precision of slow neutron capture cross section measurements using a simple moxon-rae detector. Nucl. Instrum. Methods 86 (1), 83–91, EXFOR#10501010 (Accessed on 18 October 2022), EXFOR#10501008 (Accessed on Feb. 27, 2019), EXFOR#10501009 (Accessed on Jan. 14, 2019).

Markovic, V., Kocic, A., 1971. Measurement of the thermal effective cross section and the effective resonance integral of copper and tantalum using the pile oscillator method. Bull. Boris Kidrich Inst. Nuclear Sci. 22 (1), 1, EXFOR#30289004 (Accessed on 18 October 2022).

McDermott, B.J., 2016. Resonance region capture cross section measurements in iron and tantalum using a new C_6D_6 detector array. (thesis). Rensselaer Polytechnic Institute.

McDermott, B., Blain, E., Daskalakis, A., Thompson, N., Youmans, A., Choun, H., Steinberger, W., Danon, Y., Barry, D., Block, R., et al., 2017. Ta-181 (n, γ) cross section and average resonance parameter measurements in the Unresolved Resonance Region from 24 to 1180 keV using a filtered-beam technique. Phys. Rev. C 96 (1), 014607.

Moreh, R., Block, R., Danon, Y., 2006. Generating a multi-line neutron beam using an electron linac and a U-filter. Nucl. Instrum. Methods Phys. Res. A 562 (1), 401–406.

Mughabghab, S.F., 2018. Atlas of Neutron Resonances, sixth ed. Elsevier.

Nakagawa, T., Shibata, K., Chiba, S., Fukahori, T., Nakajima, Y., Kikuchi, Y., Kawano, T., Kanda, Y., Ohsawa, T., Matsunobu, H., et al., 1995. Japanese evaluated nuclear data library version 3 revision-2: JENDL-3.2. J. Nucl. Sci. Technol. 32 (12), 1259–1271.

National Institute of Standards and Technology (NIST) Center for Neutron Research, 2022. Neutron scattering lengths and cross sections. https://www.ncnr.nist.gov/resources/n-lengths/elements/ta.html. (Accessed 30 November 2022).

Ottewitte, E., Otter, J., Rose, P., Dunford, C.L., 1971. An Evaluation of Tantalum-181 and Tantalum-182 for the ENDF/B Data File. Tech. Rep. AI-AEC-12990, North American Aviation, Inc., Canoga Park, CA (United States).

Otuka, N., Dupont, E., Semkova, V., et al., 2014. Towards a more complete and accurate experimental nuclear reaction data library (EXFOR): International collaboration between nuclear reaction data centres (NRDC). Nucl. Data Sheets 120, 272–276.

Plompen, A.J., Cabellos, O., De Saint Jean, C., et al., 2020. The joint evaluated fission and fusion nuclear data library, JEFF-3.3. Eur. Phys. J. A 56 (7), 1–108.

Pomerance, H., 1951. Thermal neutron capture cross sections. Phys. Rev. 83 (3), 641, EXFOR#11047057 (Accessed on 18 October 2022).

Prokhorov, Y., 1956. Measurement of the Effective Cross-sections of Neutron Absorption in the Middle Energy Range (thesis). EXFOR#41648011 (Accessed on 18 October 2022).

Schmunk, R., Randolph, P., Brugger, R., 1960. Total cross sections of Ti, V. Y. Ta, and W.. Nucl. Sci. Eng. 7 (2), 193–197, EXFOR#11634006 (Accessed on 18 October 2022).

Sears, V.F., 1992. Neutron Scattering Lengths and Cross Sections. Neutron News 3 (3), 26–37.

Seren, L., Friedlander, H.N., Turkel, S.H., 1947. Thermal neutron activation cross sections. Phys. Rev. 72 (10), 888, EXFOR#11447113 (Accessed on 18 October 2022).

Shibata, K., 2016. Evaluation of neutron nuclear data on tantalum isotopes. J. Nucl. Sci. Technol. 53 (7), 957–967.

Shibata, K., Iwamoto, O., Nakagawa, T., et al., 2011. JENDL-4.0: A new library for nuclear science and engineering. J. Nucl. Sci. Technol. 48 (1), 1–30. http://dx.doi.org/10.1080/18811248.2011.9711675.

Takiue, M., Ishikawa, H., 1978. Thermal neutron reaction cross section measurements for fourteen nuclides with a liquid scintillation spectrometer. Nucl. Instrum. Methods 148 (1), 157–161, EXFOR#20853013 (Accessed on 18 October 2022).

Tattersall, R., Rose, H., Pattenden, S., Jowitt, D., 1960. Pile oscillator measurements of resonance absorption integrals. J. Nuclear Energy. Part A. Reactor Sci. 12 (1–2), 32–46, EXFOR#20638056 (Accessed on 18 October 2022).

Tsubone, I., Nakajima, Y., Kanda, Y., 1987. Resonance parameters of tantalum-181 in neutron energy range from 100 to 4,300 eV. J. Nucl. Sci. Technol. 24 (12), 975–987.

Werner, C.J., Armstrong, J.C., Brown, F.B., Bull, J.S., Casswell, L., Cox, L.J., Dixon, D.A., Forster, III, R.A., Goorley, J.T., Hughes, III, H.G., Favorite, J.A., Martz, R.L., Mashnik, S.G., Rising, M.E., Solomon, Jr., C.J., Sood, A., Sweezy, J.E., Zukaitis, A.J., Anderson, C.A., Elson, J.S., Durkee, Jr., J.W., Johns, R.C., McKinney, G.W., McMath, G.E., Hendricks, J.S., Pelowitz, D.B., Prael, R.E., Booth, T.E., James, M.R., Fensin, M.L., Wilcox, T.A., Kiedrowski, B.C., 2017. MCNP User's Manual Code Version 6.2. Tech. Rep. LA-UR-17-29981, Los Alamos National Laboratory, Los Alamos, NM, USA.

Widder, F., 1975. Neutron Capture Cross Section Measurements in the Energy Region from 0.01 to 10 Electron Volts. Eidg. Inst. Reaktorforsch. Wuerenlingen Reports, EIR-217, EXFOR#20437012 (Accessed on 11 January 2019).

Wolf, G., 1960. The absolute measurement of the decay rate by means of the β-γ coincidence method and its application to the measurement of the thermal activation cross section of the isotopes Na23, Sc45, Co59, and Ta181. Nukleonik 2, 255, EXFOR#20651006 (Accessed on 18 October 2022).